

# Engineering Precise and Robust Effective Hamiltonians

Jiahui Chen<sup>1,2\*</sup> and David Cory<sup>1,3</sup>

<sup>1</sup>*Institute for Quantum Computing, Waterloo, Ontario N2L 3G1, Canada*

<sup>2</sup>*Department of Physics, University of Waterloo, Waterloo, Ontario N2L 3G1, Canada*

<sup>3</sup>*Department of Chemistry, University of Waterloo, Waterloo, Ontario N2L 3G1, Canada*

(Dated: June 27, 2025)

Engineering effective Hamiltonians is essential for advancing quantum technologies including quantum simulation, sensing, and computing. This paper presents a general framework for effective Hamiltonian engineering, enabling robust, accurate, and efficient quantum control strategies. To achieve efficiency, we focus on creating target zeroth-order effective Hamiltonians while minimizing higher-order contribution and enhancing robustness against systematic errors. The control design identifies the minimal subspace of the toggling-frame Hamiltonian and the full set of achievable, zeroth-order, effective Hamiltonians. Examples are included to illustrate the process flow and resultant precision and robustness.

## I. INTRODUCTION

Quantum processors have extraordinary potential to transform sensing, secure communication, and enhance computational efficiency, including in the simulation of quantum physics. To realize this potential, three key engineering tasks must be addressed [1–3]: (1) efficient and robust coherent control [4–9], (2) the design of complex, interconnected quantum processors [10], and (3) the implementation of quantum error correction [11]. This paper provides tools for designing coherent control methods to enhance precision and efficiency, using Average Hamiltonian Theory (AHT) as the foundational framework. Introduced by John Waugh over fifty years ago [12], AHT describes coherent averaging initially developed for NMR [13]. It has since been widely applied to decoupling [14–18], recoupling [19, 20], spectroscopy [21, 22], sensing [23, 24], quantum simulation [25, 26], multi-body physics [27–30], and quantum computing [31]. The formalism Waugh developed for the coherent control of coupled spin-1/2 particles naturally extends to the control of coupled qubits, as the control of qubits and spin-1/2 particles are isomorphic.

AHT is based on the principle that the integrated action of a time-varying total Hamiltonian,  $H_{\text{tot}}(t)$ , over a period  $[0, T_{\text{seq}})$ , can be represented by a unitary operator or, equivalently, an effective Hamiltonian,  $H_{\text{eff}}$ , and its duration,  $T_{\text{seq}}$ . The total Hamiltonian of a quantum system is typically partitioned into a user-defined, time-dependent control Hamiltonian and a time-independent internal Hamiltonian

$$H_{\text{tot}}(t) = H_c(t) + H_{\text{int}}. \quad (1)$$

The total unitary propagator is

$$\begin{aligned} U(T_{\text{seq}}) &= \mathcal{T} \exp \left( -i \int_0^{T_{\text{seq}}} H_{\text{tot}}(t) dt \right) \\ &= \exp(-i H_{\text{eff}} T_{\text{seq}}), \end{aligned} \quad (2)$$

where  $\mathcal{T}$  is the Dyson time-ordering operator, and  $H_{\text{eff}}$  is the effective Hamiltonian. When designing an effective Hamiltonian perturbatively, the most efficient solution is often achieved at zeroth order, as higher-order terms typically make increasingly smaller contributions. Methods for accounting for higher-order corrections are essential for robust applications of AHT. Table I lists common use cases of AHT, along with their goals and typical figures of merit (FoM).

To illustrate the desired outcome, consider a simple and time-independent internal Hamiltonian

$$H_{\text{int}} = \sum_{i \neq j}^N B_{ij} \vec{\sigma}_i \cdot \mathbf{D} \cdot \vec{\sigma}_j + \sum_{i=1}^N \delta_i \vec{n} \cdot \vec{\sigma}_i \quad (3)$$

where  $\vec{\sigma}_i = (\sigma_x^i, \sigma_y^i, \sigma_z^i)$  and

$$\sigma_\alpha^i = \mathbb{1}^{\otimes(i-1)} \otimes \sigma_\alpha \otimes \mathbb{1}^{\otimes(N-i)}, \quad (4)$$

for  $\alpha = \{x, y, z\}$ , are the Pauli operators acting on the  $i$ th qubit,  $B_{ij}$  are coupling strengths,  $\mathbf{D}$  is a rank-2 tensor determining the form of the qubit interactions,  $\vec{n}$  is a unit vector determining the direction,  $\delta_i$  the strength of the qubit-dependent energy offset, and  $N$  is the total number of qubits. Note that the algorithms outlined later in the paper do not depend on the particular organization of the Hamiltonians. We will show later that more complex internal Hamiltonians are easily accommodated.

In Table I, the goal of spectroscopy [32] is to measure select contributions to the internal Hamiltonian while suppressing unwanted terms. A common goal is to measure the linear terms while suppressing the bilinear terms in  $H_{\text{int}}$  [12]. The scaling factor  $s$  is preferably large and the effective direction  $\vec{v}_{\text{eff}}$  is typically chosen to be along the quantization axis. Time suspension [18, 33, 34] is

\* j562chen@uwaterloo.ca

TABLE I: Overview of applications of AHT with respective targets, goals, and FoM.

Use case	Target	Goal	FoM
Decoupling	$H_{\text{eff}} = s \sum_i \delta_i \vec{v}_{\text{eff}} \cdot \vec{\sigma}_i$	spectroscopy	line narrowing ( $\frac{1}{\pi T_2}$ ), $sT_{2x}$
Time suspension	$H_{\text{eff}} = 0$	store quantum information	decoherence ( $\frac{1}{\pi T_2}$ )
Simulation	$H_{\text{eff}} = H_{\text{sim}},$ $U(nT_{\text{seq}}) = e^{-iH_{\text{sim}}nT_{\text{seq}}}$	simulating quantum systems	$\ H_{\text{eff}} - H_{\text{sim}}\ $
Sensing	$H_{\text{eff}} = H_{\text{sen}}$	parameter estimation	Fisher information
Gates	$U(T_{\text{seq}}) = U_{\text{target}}$	computation	gate fidelity

an extension of decoupling that aims to suppress all of the terms in  $H_{\text{int}}$  so,  $H_{\text{eff}} = 0$ . It is enabling of qubit storage.  $H_{\text{sim}}$  and  $H_{\text{sen}}$  are the target effective Hamiltonians for simulation and sensing tasks. In quantum simulation, the goal is to transform  $H_{\text{int}}$  into  $H_{\text{sim}}$ , typically to explore the dynamics of the simulated system. Quantum simulation is often performed stroboscopically with  $H_{\text{sim}}(T_{\text{seq}})$  being the effective Hamiltonian over a repeated cycle of length  $T_{\text{seq}}$  and  $n$  being the index of the stroboscopic measurement. In sensing, the goal is to engineer a Hamiltonian,  $H_{\text{sen}}$ , that offers advantages, such as enhanced Fisher information, for measuring target parameters such as the strength of an external field. In gate design, the goal is to implement a target unitary  $U_{\text{target}}$  efficiently and with robustness against errors. The FoM is the gate fidelity.

Recent advances have enhanced the application of AHT. For example, J. Choi et al. [35] proposed a symmetry-based method for engineering effective Hamiltonians using control sequences composed of  $\pi/2$  pulses and delays, specifically targeting the decoupling of the zeroth-order average Hamiltonian. It enables the design of high-performance sequences for spectroscopy and quantum simulations, demonstrating superior performance compared to existing methods in the presence of strong disorders. H. Zhou et al. [36] and M. Tyler et al. [37] extended this approach to account for higher-order terms. These methods focus on control with  $\pi/2$  rotations of the qubits, anisotropic Heisenberg model, and lower-order corrections.

Reinforcement learning has been utilized to engineer effective Hamiltonians using  $\pi/2$  pulses to decouple secular dipolar interactions [38]. It has also been used to autonomously design high-fidelity quantum logic gates on superconducting systems [39]. These methods highlight the potential of advanced numerical algorithms to significantly enhance the design of sequences for Hamiltonian engineering [40].

The above methods mainly target time suspension applications. For gate design, H. Haas *et al.* [41] utilized the van Loan equation [42] to enable numerical evaluation of the Magnus expansion for control sequences. The authors further integrated their framework with GRAPE [43], facilitating efficient numerical optimization for designing sequences in Hamiltonian engineering. Other nu-

merical methods have also been proposed [44].

Several key challenges remain unresolved:

- **Controllability:** A systematic method to find the achievable set of effective Hamiltonians across different systems and controls [45] is not well-known.
- **Arbitrary control errors:** There is no general methodology for designing robust sequences that mitigate systematic errors across different control systems.
- **Higher-order decoupling:** A generic symmetry-based framework for eliminating higher-order correction terms is still lacking.

This paper aims to provide a general framework suitable for designing control sequences in the presence of control imperfections and dispersion of  $H_{\text{int}}$ . The method includes:

1. Algorithms for characterizing achievable sets of zeroth-order average Hamiltonians for any  $H_{\text{int}}$  and  $H_c$ .
2. Algorithms for finding numerically optimized sequences for engineering zero and nonzero effective Hamiltonians.
3. Method to reduce the effects of most systematic errors in the control system.
4. Method to reduce higher-order corrections from the Magnus expansion.

## II. EFFECTIVE HAMILTONIAN ENGINEERING AND TOGGLING FRAME

For robust control, the internal and control Hamiltonians are broken up into isochromats that describe the range of possible parameters. For each isochromat, the control is unitary so an effective Hamiltonian (Eq. 2) always exists. For the dynamics averaged over a distribution of isochromats, the overall map is a convex sum of unitary processes and so is a completely positive trace-preserving (CPTP) map. The effective Hamiltonian ( $H_{\text{eff}}$ ) is formally calculated by taking the matrix

logarithm of  $U(T_{\text{seq}})$ .  $H_{\text{eff}}$  describes the system's effective dynamics over the interval  $[0, T_{\text{seq}})$  and is not unique since adding integer multiples of  $2\pi$  to its eigenvalues yields the same unitary  $U(T_{\text{seq}})$ . In place of matrix logarithm, AHT often uses a perturbative series approximation to evaluate  $H_{\text{eff}}$  via the Magnus expansion:

$$H_{\text{eff}}(T_{\text{seq}}) = \sum_{n=0}^{\infty} \bar{H}^{(n)}(T_{\text{seq}}), \quad (5)$$

where  $n$  is the perturbation order, and  $\bar{H}^{(n)}$  is the  $n$ th-order average Hamiltonian. The zeroth-order average Hamiltonian is

$$\bar{H}^{(0)}(T_{\text{seq}}) = \frac{1}{T_{\text{seq}}} \int_0^{T_{\text{seq}}} H_{\text{tot}}(t) dt. \quad (6)$$

For the special case when the total Hamiltonian commutes with itself at all times,  $H_{\text{eff}}(T_{\text{seq}}) = \bar{H}^{(0)}(T_{\text{seq}})$ . We are interested in the general case, where we focus on finding a control sequence such that

$$H_{\text{target}} = \bar{H}^{(0)}(T_{\text{seq}}). \quad (7)$$

Having a zeroth-order average Hamiltonian implementation of  $H_{\text{target}}$  is advantageous since when a solution is achievable in the zeroth order, it is typically the most efficient implementation in terms of resources such as the power bandwidth product. If  $H_{\text{target}}$  is achievable in zeroth order, a good strategy is to find a control sequence achieving Eq. (7) while individually minimizing each residual higher-order term in the Magnus expansion:

$$\bar{H}^{(1)}(T_{\text{seq}}), \bar{H}^{(2)}(T_{\text{seq}}), \dots \quad (8)$$

Of course, not all potential  $H_{\text{target}}$  are achievable in zeroth order. Engineering higher-order terms will be addressed in a different paper.

The toggling frame is a powerful tool that simplifies finding average Hamiltonians. It bridges numerical integration and perturbative expansion by partitioning  $H_{\text{tot}}(t)$  into a primary part and a perturbative part:

$$H_{\text{tot}}(t) = H_{\text{pri}}(t) + H_{\text{pert}}(t). \quad (9)$$

The toggling frame is the interaction frame of  $H_{\text{pri}}(t)$ . A common use of AHT is to take the control Hamiltonian  $H_c$  as  $H_{\text{pri}}$  and the internal Hamiltonian  $H_{\text{int}}$  as  $H_{\text{pert}}$ . This restriction, however, is unnecessary, and the freedom to choose any partition of  $H_{\text{tot}}$  enables a larger set of achievable controls in zeroth order. The toggling-frame Hamiltonian of  $H_{\text{pert}}(t)$  is

$$H_{\text{tog}}(t) = U_{\text{pri}}^\dagger(t) H_{\text{pert}}(t) U_{\text{pri}}(t), \quad (10)$$

where the primary unitary  $U_{\text{pri}}(t)$  is

$$U_{\text{pri}}(t) = \mathcal{T} \exp\left(-i \int_0^t H_{\text{pri}}(t') dt'\right). \quad (11)$$

The perturbative unitary is

$$\begin{aligned} U_{\text{pert}}(T_{\text{seq}}) &= \mathcal{T} \exp\left(-i \int_0^{T_{\text{seq}}} H_{\text{tog}}(t) dt\right) \\ &= \exp(-i H_{\text{eff}} T_{\text{seq}}). \end{aligned} \quad (12)$$

Then, the total propagator is

$$U(T_{\text{seq}}) = U_{\text{pri}}(T_{\text{seq}}) U_{\text{pert}}(T_{\text{seq}}), \quad (13)$$

where  $U_{\text{pri}}$  and  $U_{\text{pert}}$  can be evaluated through numerical integration and perturbative expansion, respectively.

### III. CONTROL SETUP

The control Hamiltonian is most often implemented as a sequence of piecewise constant intervals of control parameters  $\{a_k(t)\}$ . For example, it can be

$$\begin{aligned} H_c(t) &= \sum_{i=1}^N [\omega_1^i(t) \cos(\phi_i(t)) \sigma_x^i + \omega_1^i(t) \sin(\phi_i(t)) \sigma_y^i \\ &\quad + (\omega_0 - \omega_r^i(t)) \sigma_z^i], \end{aligned} \quad (14)$$

where the time-dependent amplitude ( $\omega_1^i(t)$ ), frequency ( $\omega_r^i(t)$ ) and phase of the control field ( $\phi_i(t)$ ) on the  $i$ th qubit are control parameters ( $a_k(t)$ ).  $a_k(t)$  is typically set to zero at the beginning and the end of each sequence [40], enabling a simple composition of gates.

The control system (Fig. 1) maps  $\{a_k(t)\}$  to a continuous output field  $\vec{B}(t)$  that is conveniently described in the lab frame. This map is generally a non-invertible, smooth, nonlinear function depending on time-independent parameters of the control system,  $\{\mu_j\}$ , such as reactance, spatial and temporal variations of control fields, nonlinearities from kinetic inductance, etc. Variations in  $\{\mu_j\}$  result in a modification of the control Hamiltonian by an error Hamiltonian  $\Delta H$ . The error Hamiltonian  $\Delta H$  can be evaluated by applying the Taylor expansion to the map from  $\{a_k(t)\}$  to  $\vec{B}(t)$  with respect to  $\{\mu_j\}$ . Robustness to variations in  $\{\mu_j\}$  can then be achieved by minimizing the effective Hamiltonian of  $\Delta H$ . The following methods are capable of finding high-precision control fields that account for  $\{\mu_j\}$  and are robust to their variations.

The internal Hamiltonian also depends on a set of parameters,  $\{\eta_{\text{int}}^i\}$ , which can include terms such as the Zeeman splitting, chemical shift, coupling strengths, etc. Typically,  $\{\eta_{\text{int}}^i\}$  are governed by a classical probability distribution with a correlation time that is often longer than the total length of a control cycle ( $T_{\text{seq}}$ ).

Given a sequence  $\{a_k(t)\}$ , as well as the internal and model parameters ( $\{\eta_{\text{int}}^i\}$  and  $\{\mu_j\}$ ), the density matrix

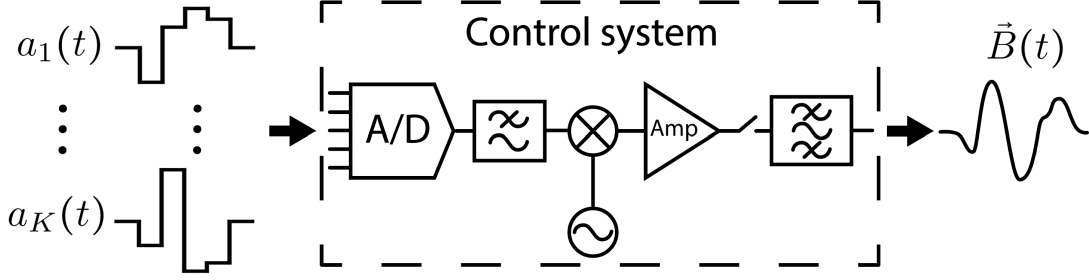


FIG. 1: Illustration of a very simplified control system. The input signals  $\{a_k(t)\}$  are designed by the user. The control system outputs a continuous control field  $\vec{B}(t)$  acting on the qubit system in the lab frame. The design of  $\{a_k(t)\}$  should account for the model of the system so that it captures the distortion of the hardware along with additive noise. In this case, the control parameters  $a_k(t)$  are transformed via convolution with a kernel reflecting the bandwidth of the low- and band-pass filters. More complete mappings are explored in Sec. V C.

of the system obeys the master equation

$$\frac{d}{dt}\rho(t) = -i[H_{\text{tot}}(\{a_k(t)\}; \{\mu_j\}, \{\eta_{\text{int}}^i\}), \rho(t)] + \mathcal{L}_{\text{relaxation}}[\rho(t)] \quad (15)$$

where  $\mathcal{L}_{\text{relaxation}}$  is the Lindbladian for relaxation. The solution to Eq. (15) over the interval  $[0, T_{\text{seq}}]$  is

$$\rho(T_{\text{seq}}) = \Lambda(\{a_k(t)\}; \{\mu_j\}, \{\eta_{\text{int}}^i\})(\rho_0), \quad (16)$$

where  $\rho_0$  is the initial density matrix and  $\Lambda(\{a_k(t)\}; \{\mu_j\}, \{\eta_{\text{int}}^i\})$  is a CPTP map. The density matrix of the system for an expectation-valued measurement is the ensemble average of Eq. (16) over the distributions of  $\{\mu_j\}$  and  $\{\eta_{\text{int}}^i\}$ :

$$\bar{\rho}(T_{\text{seq}}) = \bar{\Lambda}(\rho_0), \quad (17)$$

where the average CPTP map  $\bar{\Lambda}$  is

$$\bar{\Lambda} = \int d\{\mu_j\} d\{\eta_{\text{int}}^i\} p(\{\mu_j\}) p(\{\eta_{\text{int}}^i\}) \Lambda(\{a_k(t)\}; \{\mu_j\}, \{\eta_{\text{int}}^i\}). \quad (18)$$

The goal is to design  $\{a_k(t)\}$  to achieve the desired FoM with respect to [46]  $\bar{\Lambda}$  or  $\bar{\rho}(T_{\text{seq}})$  for tasks in Table 1. For example, if the overall unitary target for  $U(T_{\text{seq}})$  is  $U_0$ , then the average gate fidelity of the sequence can be calculated as

$$\mathcal{F}_{\text{ave}}(\{a_k(t)\}, U_0) = \int \langle \psi | U_0^\dagger \bar{\Lambda}(|\psi\rangle\langle\psi|) U_0 | \psi \rangle d\psi. \quad (19)$$

When knowing the details of the errors is important (e.g., in implementing quantum error correction, noiseless subsystems, and distinguishing between coherent and stochastic errors), one should report the full average CPTP map  $\bar{\Lambda}$ . Note that since the FoM and the CPTP map  $\bar{\Lambda}$  are typically estimated via Monte Carlo simulations, they are not suitable for direct use in the design

of control sequences. Instead, a simple overlap is used to estimate the fidelity of  $U(T_{\text{seq}})$ :

$$\mathcal{F}(U(T_{\text{seq}}), U_0) = \frac{|\text{Tr}(U(T_{\text{seq}})^\dagger U_0)|}{\text{Tr}(U_0^\dagger U_0)}. \quad (20)$$

This definition is also used for plotting the control landscapes.

#### IV. FLOWCHART FOR EFFECTIVE HAMILTONIAN ENGINEERING

The design method is given as a flowchart which references algorithms that are provided in pseudocode. The flowchart is the same for all applications in Table I.

1. Describe the quantum system and controls:
  - (a) Provide a description of  $H_{\text{int}}$  including distributions of  $\{\eta_{\text{int}}^i\}$ .
  - (b) Provide a description of  $H_c(t)$  and a model of the control system including finite bandwidth, maximal power, and nonlinearities and distributions of the model parameters  $\{\mu_j\}$ . Specify the error Hamiltonian  $\Delta H$ .
  - (c) Provide relaxation times when desired.
2. Identify from Table 1 the use case and its objectives. Partition  $H_{\text{tot}}$  into  $H_{\text{pri}}$  and  $H_{\text{pert}}$  accordingly. Specify the target unitary  $U_{\text{target}}$  and/or effective Hamiltonian  $H_{\text{target}}$  and the required FoM.
3. Determine the controllability of  $U(T_{\text{seq}})$ :
  - (a) Controllability of  $U_{\text{pri}}$ : Use Algorithm 1 to determine if  $U_{\text{target}}$  is achievable.
  - (b) Space of achievable  $\vec{H}^{(0)}$ : Use Algorithm 2 to determine if  $H_{\text{target}}$  is in the space of achievable zeroth-order average Hamiltonians ( $\vec{H}^{(0)}$ ).

- (c) Range of achievable scaling factors for  $H_{\text{target}}$ : Use Algorithm 3 to check if  $sH_{\text{target}}$  is achievable. If yes, set  $H_{\text{target}} \leftarrow sH_{\text{target}}$ .
- (d) If  $U_{\text{pri}}$  or  $sH_{\text{target}}$  are not achievable, go to Step 1 to change  $H_c(t)$  if additional control is available in the physical system. Sometimes (see below for an explanation of **Step 3** (d)), one can go to Step 2 to choose a different partitioning to enable a larger set of achievable  $\bar{H}^{(0)}$ .
4. Using a numerical optimizer to find a control sequence that maximizes the FoM targets. The FoM targets are achieved by reaching the desired precision in  $U_{\text{pri}}(T_{\text{seq}}) \leftarrow U_{\text{target}}$  and  $\bar{H}^{(0)} \leftarrow H_{\text{target}}$  while accounting for the model of the control system, minimizing sensitivity to variations in the  $\{\mu_j\}$  and  $\{\eta_{\text{int}}^i\}$ , and removing higher-order corrections  $\bar{H}^{(1)}, \bar{H}^{(2)}, \dots$
5. Calculate the control landscape, accounting for relaxation and the full model of the control system. Check if the desired FoM and robustness are reached. If yes, return the sequence. Otherwise, if the FoM is low due to relaxation, go to Step 3 (c) to choose a larger  $s$ . If the robustness is not sufficient, go to Step 4 to include higher-order robustness.

The following sections expand upon the flowchart step by step.

### Step 1. Description of the quantum system and controls

(a) *Description of  $H_{\text{int}}$ .* The description of  $H_{\text{int}}$  includes the operators, amplitudes and distributions of  $\{\eta_{\text{int}}^i\}$ . For example, for  $H_{\text{int}}$  in Eq. (3), one needs to specify  $\mathbf{D}$  and  $\bar{n}$ , distributions of the coupling strengths ( $B_{ij}$ ) and the offsets ( $\delta_i$ ), usually obtained via spectroscopy.

(b) *Description of  $H_c(t)$ .* The description of  $H_c(t)$  includes the input parameters  $\{a_k(t)\}$  and a mapping, given by the model of the control system, that maps  $\{a_k(t)\}$  to the output field  $\vec{B}(t)$  in the lab frame. The map is generally given as first-order state-space differential equations. For time-invariant linear systems, the map is determined by the transfer function. Once a map from  $\{a_k(t)\}$  to  $\vec{B}(t)$  is given,  $H_c(t)$  is obtained by moving into the reference frame of the qubits. The distributions of the model parameters  $\{\mu_j\}$  (obtained via “tune-up” cycles [47]) can be included. The error Hamiltonian  $\Delta H$  is obtained by expanding the map from  $\{a_k(t)\}$  to  $\vec{B}(t)$  with respect to  $\{\mu_j\}$ .

(c) *Relaxation time.* Provide an estimate of relaxation times. Typically,  $T_1$  and  $T_2$  are included. When available,  $T_{1\rho}$  can be included.  $T_2^*$  is best included in the distribution of qubit energies. Alternatively, one can use

quantum process tomography to determine the full system Lindbladian [48].

### Step 2. Define partitioning of $H_{\text{tot}}$ and objectives

The partitioning of  $H_{\text{tot}}$  is for computational convenience, enabling an efficient use of the toggling frame to determine average Hamiltonians. Default partitioning is  $H_{\text{pri}} = H_c + H_{\text{int}}$  and  $H_{\text{pert}}$  includes variations in  $H_{\text{int}}$ , as in gate design and simulation and sensing when the Lie algebra of the system can be calculated exactly. For decoupling and time suspension, and simulation and sensing with large systems or when one wants to control the rate of the dynamics,  $H_{\text{int}}$  can be included in  $H_{\text{pert}}$  and engineered perturbatively.

Specify  $U_{\text{target}}$ ,  $H_{\text{target}}$  and  $T_{\text{seq}}$ . Choose target fidelity for the process. Verify that for the relaxation time and  $T_{\text{seq}}$  the target FoM is achievable.

### Step 3. Controllability of $U_{\text{pri}}$

(a) *Controllability of  $U_{\text{pri}}$ .* The controllability of  $U_{\text{pri}}$  is found by calculating the minimal Lie algebra containing  $H_{\text{pri}}(t)$ . For example, the Lie algebra is  $\mathfrak{g}_{\text{pri}} = \text{span}_{\text{Lie}}\{\sigma_x, \sigma_y, \sigma_z\}$  for universal control on a single qubit and the set of Hamiltonians is the generators of  $\mathfrak{g}_{\text{pri}}$ . The corresponding Lie group  $e^{\mathfrak{g}_{\text{pri}}} = \{e^g | g \in \mathfrak{g}_{\text{pri}}\}$  gives the set of achievable  $U_{\text{pri}}(T_{\text{seq}})$  [45] and states [49]. Given a set of generators  $\{H_i\}$ , Algorithm 1 calculates the generated Lie algebra [45].

---

**Algorithm 1** Algorithm for calculating the Lie algebra generated by  $\{H_i\}$ . The function FINDLIEALGEBRA( $\{H_i\}$ ) takes a set of generators  $\{H_i\}$  and returns an orthonormal basis of the generated Lie algebra.

---

```

1: function FINDLIEALGEBRA( $\{H_i\}$ )
2:    $\mathcal{A}_0 \leftarrow \{H_i\}$ 
3:    $v \leftarrow 0$ 
4:   while  $\mathcal{A}_v$  is not empty and  $|\cup_{i=1}^v \mathcal{A}_i| < 2^{2N} - 1$  do  $\triangleright$ 
      $2^{2N}$  is the dimension of the Hilbert space
5:      $\mathcal{A}_{v+1} \leftarrow \{\}$ 
6:     for  $g \in \mathcal{A}_0$  and  $h \in \mathcal{A}_v$  do
7:       if  $[h, g]$  is linearly independent with  $\cup_{i=1}^{v+1} \mathcal{A}_i$ 
         then  $\triangleright$  Linear dependence can be checked by
           calculating the rank of the matrix of the vectorizations of
           the operators.
8:           Append  $[h, g]$  to  $\mathcal{A}_{v+1}$ 
9:       end if
10:    end for
11:     $v \leftarrow v + 1$ 
12:  end while
13:  Use the Gram–Schmidt process to orthonormalize
      $\cup_{i=1}^v \mathcal{A}_i$  and return the result.
14: end function

```

---

(b) *Minimal Subspace of  $H_{\text{tog}}(t)$ .* The minimal subspace containing the toggling-frame Hamiltonian is also

the subspace of achievable zeroth-order average Hamiltonians. It is

$$\mathcal{C}(\mathbf{g}_{\text{pri}}, H_{\text{pert}}) = \text{span}_{\mathbb{R}} \{U_{\text{pri}}^\dagger(t)H_{\text{pert}}U_{\text{pri}}(t) | U_{\text{pri}}(t) \in e^{\mathbf{g}_{\text{pri}}}\}. \quad (21)$$

Since  $H_{\text{tog}}(t)$  is determined by the action of  $H_{\text{pri}}(t)$  on  $H_{\text{pert}}$ , the subspace can be calculated by taking nested commutators between  $\mathbf{g}_{\text{pri}}$  and  $H_{\text{pert}}$ :

$$\mathcal{C}(\mathbf{g}_{\text{pri}}, H_{\text{pert}}) = \text{span}_{\mathbb{R}} \{[g_1, \dots [g_L, H_{\text{pert}}] \dots] | g_l \in \mathbf{g}_{\text{pri}}, L \geq 0\}. \quad (22)$$

Algorithm 2 calculates an orthonormal basis of  $\mathcal{C}(\mathbf{g}_{\text{pri}}, H_{\text{pert}})$ :

---

**Algorithm 2** Algorithm for calculating an orthonormal basis of  $\mathcal{C}(\mathbf{g}_{\text{pri}}, H_{\text{pert}})$ . The function  $\text{FINDC}(\mathcal{B}(\mathbf{g}_{\text{pri}}), H_{\text{pert}})$  takes as input a basis  $\mathcal{B}(\mathbf{g}_{\text{pri}}) = \{e_1, \dots, e_{|\mathbf{g}_{\text{pri}}|}\}$  of  $\mathbf{g}_{\text{pri}}$  and the operator  $H_{\text{pert}}$ , and returns an orthonormal basis of  $\mathcal{C}(\mathbf{g}_{\text{pri}}, H_{\text{pert}})$ .

---

```

1: function FINDC( $\mathcal{B}(\mathbf{g}_{\text{pri}}), H_{\text{pert}}$ )
2:    $b_1 \leftarrow H_{\text{pert}}$ 
3:    $i_{\text{max}} \leftarrow 1$  ▷ Total number of basis vectors.
4:    $i_{\text{new}} \leftarrow 1$  ▷ Number of new basis vectors.
5:   while  $i_{\text{new}} > 0$  and  $i_{\text{max}} \leq 2^{2N} - 1$  do
6:      $t \leftarrow 0$ 
7:     for  $i_{\text{max}} - i_{\text{new}} + 1 < i < i_{\text{max}}$  do
8:       for  $1 < j < |\mathbf{g}_{\text{pri}}|$  do
9:         if  $b_1, \dots, b_{i_{\text{max}}+t}, [e_j, b_i]$  are linearly independent then
10:            $t \leftarrow t + 1$ 
11:            $b_{i_{\text{max}}+t} \leftarrow [e_j, b_i]$ 
12:         end if
13:       end for
14:     end for
15:      $i_{\text{max}} \leftarrow i_{\text{max}} + t$ 
16:      $i_{\text{new}} \leftarrow t$ 
17:   end while
18:   Use the Gram–Schmidt process to orthonormalize
   ( $b_1, \dots, b_{i_{\text{max}}}$ ) and return the result
19: end function

```

---

(c) *Achievable range of scaling factors.* The set of achievable  $\bar{H}^{(0)}(T_{\text{seq}})$  is

$$\mathcal{O}'(\mathbf{g}_{\text{pri}}, H_{\text{pert}}) = \left\{ \frac{1}{T_{\text{seq}}} \int_0^{T_{\text{seq}}} U_{\text{pri}}^\dagger(t)H_{\text{pert}}U_{\text{pri}}(t)dt \right\}. \quad (23)$$

It is the convex hull of  $\{U_i^\dagger H_{\text{pert}} U_i\}$  ( $U_i \in e^{\mathbf{g}_{\text{pri}}}$ ), which can be approximated through random sampling [50]. Therefore, along each  $H_{\text{target}} \in \mathcal{C}(\mathbf{g}_{\text{pri}}, H_{\text{pert}})$ , the range of achievable scaling factors can be found by solving a linear program associated with the sampled set (Fig. 2). The procedure is summarized in Algorithm 3.

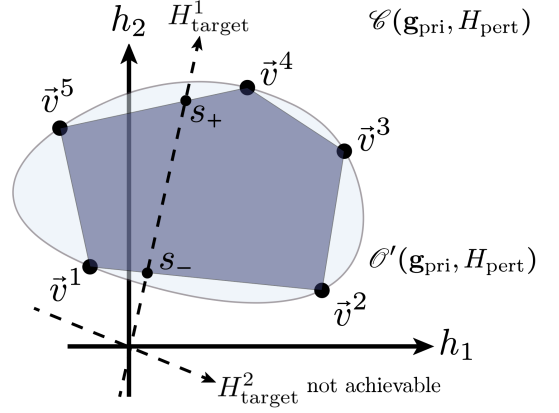


FIG. 2: Schematic for finding achievable scaling factors. The set of achievable zeroth-order average Hamiltonians  $\mathcal{O}'(\mathbf{g}_{\text{pri}}, H_{\text{pert}})$  (light blue area) is a convex set in  $\mathcal{C}(\mathbf{g}_{\text{pri}}, H_{\text{pert}})$  (spanned by  $h_1$  and  $h_2$ ). The convex set is approximated by the polygon (dark blue area) formed by  $\{\tilde{v}_i = U_i^\dagger H_{\text{pert}} U_i\}$ . The achievable scaling factors for  $H_{\text{target}}$  can then be found via linear programming.

---

**Algorithm 3 (informal version)** Algorithm for finding the range of achievable scaling factors for  $H_{\text{target}}$ .

---

```

1: Sample random unitaries  $U_i \in e^{\mathbf{g}_{\text{pri}}}$  to form the set
    $\{U_i^\dagger H_{\text{pert}} U_i\}$ 
2: Solve the linear program that maximizes (minimizes) the
   projection of the convex combination of  $\{U_i^\dagger H_{\text{pert}} U_i\}$  onto
    $H_{\text{target}}$ ; the solution corresponds to  $s_+$  ( $s_-$ )
3: return  $[s_-, s_+]$  as the range of achievable scaling factors

```

---

Note, linear programming has been used previously to find optimal scaling factors and pulse sequences for Hamiltonian engineering in a filtering space [51].

(d) *Modify control or partitioning:* For gate design, simulation and sensing where  $H_{\text{pri}} = H_c + H_{\text{int}}$ , spectroscopy, and decoupling, if  $U_{\text{target}}$  or  $sH_{\text{target}}$  are not achievable, one needs to introduce additional control fields (e.g., RF, microwave, or laser fields) to modify the controllability. For simulation and sensing where  $H_{\text{pert}}$  includes  $H_{\text{int}}$ , one can put part of  $H_{\text{int}}$  in  $H_{\text{pri}}$  to modify controllability of  $U_{\text{pri}}$  and  $\bar{H}^{(0)}$ .

#### Step 4. Find locally optimized sequence

Given the relaxation times and desired FoM, determine the maximal  $T_{\text{seq}}$  of a sequence that allows the target FoM. Specify higher-order corrections including higher-order terms in the Magnus expansion of  $\Delta H$  and  $H_{\text{pert}}$  and their cross terms. Use a numerical optimizer, such as gradient descent [43] or simulated annealing [52], to find  $\{a_k(t)\}$  that achieves  $U_{\text{target}}$  and  $H_{\text{target}}$  within the desired fidelity while accounting for designated error terms and higher-order corrections. A solution should be searched with short  $T_{\text{seq}}$  first and with an increased  $T_{\text{seq}}$

if no solution can be found with the current value of  $T_{\text{seq}}$  so that shorter sequences can be found.

### Step 5. Estimate sequence performance

The control landscape is obtained by calculating the fidelity between  $U(T_{\text{seq}})$  and target total unitary  $U_0$  for each set of values of  $\{\mu_j\}$  and  $\{\eta_{\text{int}}^i\}$  drawn from their respective distributions. Simulate the resulting average CPTP map  $\bar{\Lambda}$  and/or the average density matrix  $\bar{\rho}(T_{\text{seq}})$  of the system (Eq. (18)) using, e.g., the Monte Carlo method. Calculate FoM through either the average gate fidelity (Eq. (19)) or the state fidelity  $\text{Tr}(\sqrt{\sqrt{\rho_{\text{target}}}\bar{\rho}(T_{\text{seq}})\sqrt{\rho_{\text{target}}}})^2$ . If the FoM is unsatisfactory, check  $\bar{\Lambda}$  to identify the error. If the error is due to a depolarization, check if  $T_{\text{seq}}$  is too long. If not, then the robustness is insufficient, go to Step 4 to include higher-order corrections involving  $\Delta H$  and variations of  $H_{\text{int}}$ . If the error is coherent, go to Step 4 to increase target fidelity or include higher-order corrections.

## V. EXAMPLES

We now present examples to demonstrate the power of the method to achieve robustness to control errors and variations in  $H_{\text{int}}$ , characterize controllability, design effective Hamiltonians, and incorporate higher-order corrections. We explore the application of the method in gate design, quantum simulation, and sensing.

### A. Robust Hadamard

We design a Hadamard gate that is robust to variations in the Rabi field strength and offset. This sequence is useful for high-fidelity quantum operations in NMR, ESR, trapped-ion, quantum dot, Rydberg atom, and superconducting systems.

Step 1. System and controls. The internal and control Hamiltonians are

$$\begin{aligned} H_{\text{int}} &= \omega_0 \sigma_z, \\ H_c(t) &= \omega_1(t) \cos(\omega_r t + \phi(t)) \sigma_x, \end{aligned} \quad (24)$$

where, for this example, we choose  $\omega_0 = 1$  GHz ( $1 \text{ Hz} = 2\pi \text{ rad}\cdot\text{s}^{-1}$ ) as the resonance frequency of the qubit,  $\omega_r$  as the transmitter microwave frequency. The control parameters are the amplitude of the applied microwave field ( $\omega_1(t)$ ) and its phase ( $\phi(t)$ ). The maximal value of  $\omega_1(t)$  is 20 MHz. The control system has a 500 MHz bandwidth.

It is convenient to move to an interaction frame that rotates at the transmitter frequency  $\omega_r$  and take the rotating wave approximation [53]. The internal and control

Hamiltonians in this frame are

$$\begin{aligned} H_{\text{int}} &= \Delta\omega \sigma_z, \\ H_c(t) &= \omega_1(t) [\cos(\phi(t)) \sigma_x + \sin(\phi(t)) \sigma_y], \end{aligned} \quad (25)$$

where  $\Delta\omega = \omega_0 - \omega_r$  is the offset.

The gate is designed to be robust to variations in the amplitude of the applied microwave field, where the amplitude is  $(1 + \epsilon)\omega_1(t)$  where  $\epsilon$  is a random variable sampled from a uniform distribution  $\text{Unif}[-5\%, 5\%]$ . Thus, the error Hamiltonian is  $\Delta H(t) = \epsilon H_c(t)$ . The gate is also designed to be robust to variations in  $\Delta\omega$ , sampled from  $\text{Unif}[-2.5 \text{ MHz}, 2.5 \text{ MHz}]$ .

The qubit decoherence is modeled as a depolarizing channel with a characteristic time of 100 ms.

Step 2. Objectives and partitioning of  $H_{\text{tot}}$ . Choose the partitioning  $H_{\text{pri}} = H_c(t)$  and  $H_{\text{pert}} = H_{\text{int}}$ . The objectives are

$$U_{\text{target}} = \frac{1}{\sqrt{2}} \begin{pmatrix} 1 & 1 \\ 1 & -1 \end{pmatrix}. \quad (26)$$

and  $H_{\text{target}} = 0$ . The target FoM is 0.9999.

Step 3. Controllability. The set of generators of  $\mathbf{g}_{\text{pri}}$  is  $\{\sigma_x, \sigma_y\}$ , and their composition via Algorithm 1 provides universal control over the qubit space. Therefore,  $U_{\text{target}}$  is achievable. Using Algorithm 2, an orthonormal basis of  $\mathcal{C}(\mathbf{g}_{\text{pri}}, H_{\text{int}})$  is  $\{\sigma_x, \sigma_y, \sigma_z\}/\sqrt{2}$ . Choose  $H_{\text{target}} = s\sigma_z/\sqrt{2}$ . Via Algorithm 3, the range of achievable scaling factors is  $[-1, 1]$ . Therefore,  $H_{\text{target}} = 0$  is achievable in zeroth order.

Step 4. Design robust sequence. The target gate fidelity is 0.9999, so given the strength of the depolarizing channel, the maximum gate time  $T_{\text{seq}}$  is 10  $\mu\text{s}$ . Within this range, the number of intervals can be varied until the target fidelity is achieved. Here, results are shown for a sequence with 35 intervals and  $T_{\text{seq}} = 0.35 \mu\text{s}$ . The higher-order terms to minimize in the Magnus expansion include the first-order corrections of  $\Delta H$  and  $H_{\text{int}}$ , with their cross term. A generalized simulated annealing optimizer [52, 54] is used to search for an optimized sequence. The sequence and its control landscape are shown in Fig. 3. For comparison, the control landscapes of a non-robust sequence with the same  $T_{\text{seq}}$  are also shown.

Step 5. Calculate FoM. To simulate the FoM, assume  $\epsilon \sim \mathcal{N}(0, 0.01^2)$ , i.e., a normal distribution with zero mean and variance  $0.01^2$  and that  $\Delta\omega \sim \mathcal{N}(0, (0.5\text{MHz})^2)$ . The average gate fidelity (Eqs. (17) and (18)) of the resulting CPTP map of the robust and non-robust sequences are estimated to be  $0.99990_{-0.00004}^{+0.00009}$  and  $0.994_{-0.003}^{+0.005}$  where the error bars correspond to the 20th and 80th percentiles. The FoM satisfies the requirement of being at least 0.9999. The performance of the robust and non-robust sequences can also be compared by calculating the average CPTP maps using Eq. (18). The representations under the basis  $\{\mathbb{1}, \sigma_x, \sigma_y, \sigma_z\}/\sqrt{2}$

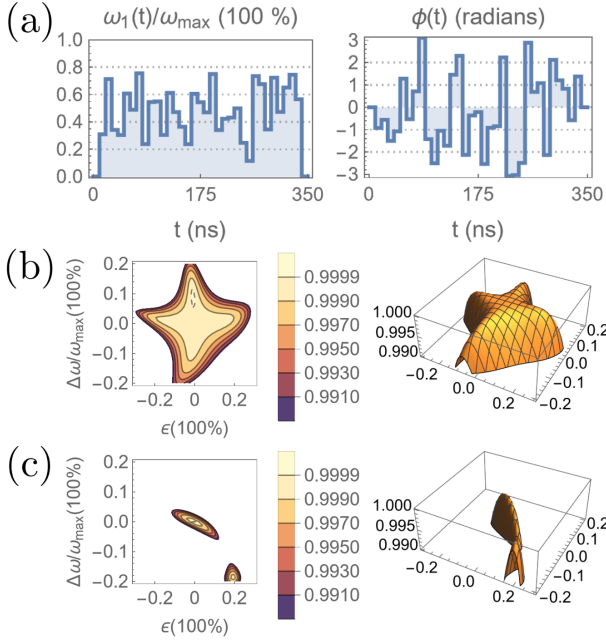


FIG. 3: (a) Control parameters of a Hadamard gate that is robust to Rabi and offset variations. (b) Contour and 3D landscapes of fidelity for the robust sequence. (c) Same as (b), but for a non-robust Hadamard gate of the same  $T_{\text{seq}}$ .

are

$$\bar{\Lambda}_{\text{robust}} = \begin{pmatrix} 1 & & \\ & 0.0329 & 0.0036 & 0.9994 \\ & -0.0076 & -0.9999 & 0.0039 \\ & 0.9994 & -0.0077 & -0.0329 \end{pmatrix}, \quad (27)$$

$$\bar{\Lambda}_{\text{non-robust}} = \begin{pmatrix} 1 & & \\ & 0.0101 & 0.0067 & 0.9708 \\ & 0.0089 & -0.9865 & 0.0240 \\ & 0.9747 & 0.0336 & -0.0227 \end{pmatrix}.$$

The low FoM of the non-robust sequence is mainly due to its poor robustness rather than a unitary error. Averaging over parameter distributions typically causes depolarization of the density matrix. In general, the coherence of the error can be measured by the orthogonality of  $\bar{\Lambda}$ :

$$\mathcal{R}(\bar{\Lambda}) = \frac{\bar{\Lambda}^T \bar{\Lambda}}{\dim(\bar{\Lambda})}. \quad (28)$$

A small orthogonality indicates insufficient robustness. For the two CPTP maps above, we have  $\mathcal{R}(\bar{\Lambda}_{\text{robust}}) = 0.99993$  and  $\mathcal{R}(\bar{\Lambda}_{\text{non-robust}}) = 0.96703$ .

## B. Robust Hadamard with finite control bandwidth

Here, we add distortion to the Hadamard control sequence from having a finite bandwidth (80 MHz) in a linear control system. The gate is designed to be robust

to variations in bandwidth and to small anti-symmetric phase transients. For a square pulse, anti-symmetric phase transients refer to quadrature components at the leading and trailing edges with equal amplitude but opposite phase.

**Step 1. System and controls.** In the rotating frame ( $\omega_0 = \omega_r = 1$  GHz), the internal and control Hamiltonians are

$$\begin{aligned} H_{\text{int}} &= 0, \\ H_c(t) &= B_x(t)\sigma_x + B_y(t)\sigma_y, \end{aligned} \quad (29)$$

where  $B_x(t)$  and  $B_y(t)$  are the time-dependent  $x$  and  $y$  components of the control field in the rotating frame. The control parameters are  $\omega_1(t)$  (maximal value is 20 MHz) and  $\phi(t)$  ( $H_c(t)$  in Eqs. (25)), they are mapped to  $\vec{B}(t)$  via a convolution with a kernel  $\Phi$

$$\begin{pmatrix} B_x(t) \\ B_y(t) \end{pmatrix} = \Phi \star \begin{pmatrix} \omega_1(t) \cos(\phi(t)) \\ \omega_1(t) \sin(\phi(t)) \end{pmatrix}, \quad (30)$$

with

$$\Phi = \begin{pmatrix} \phi^A & \phi^P \\ -\phi^P & \phi^A \end{pmatrix}. \quad (31)$$

$\phi^A$  and  $\phi^P$  represent the amplitude and phase responses of the system respectively:

$$\phi^A = \begin{cases} W e^{-Wt} & t > 0 \\ 0 & t \leq 0 \end{cases} \quad \text{and} \quad \phi^P = \begin{cases} \delta(1 - Wt) e^{-Wt} & t > 0 \\ 0 & t \leq 0 \end{cases}. \quad (32)$$

Here, the bandwidth  $W$  and  $\delta = \omega^* - 1$  GHz are the model parameters, and  $\omega^*$  is the free ringing frequency of the system. For a series RLC circuit,  $\omega^* = \sqrt{\frac{1}{LC} - \left(\frac{R}{2L}\right)^2}$ . The distortion given by the kernel  $\Phi$  is discussed in detail in [55, 56].  $W$  and  $\delta$  are random variables that follow  $W \sim \text{Unif}[70, 90]$  MHz and  $\delta \sim \text{Unif}[-20, 20]$  MHz. The leading-order approximation of the error Hamiltonian is

$$\Delta H \approx (W - 80 \text{ MHz}) \frac{\partial H_c}{\partial W} (W = 80 \text{ MHz}) + \delta \frac{\partial H_c}{\partial \delta} (\delta = 0). \quad (33)$$

**Steps 2 and 3** Since  $H_{\text{int}} = 0$ , no  $H_{\text{target}}$  is needed here. The rest of the steps are the same as in the example above.

**Step 4. Robustness and optimization.** Similar to the previous example, we design for a fidelity of 0.9999 or higher, and the maximum gate time  $T_{\text{seq}}$  is 10  $\mu\text{s}$ . Robustness to  $\Delta H$  is achieved by minimizing the zeroth-order average Hamiltonians of  $\frac{\partial H_c}{\partial W}$  and  $\frac{\partial H_c}{\partial \delta}$  simultaneously. Fig. 4 shows an optimized sequence ( $T_{\text{seq}} = 180$  ns) and its control landscape. As a comparison, the control landscape of a non-robust sequence with the same  $T_{\text{seq}}$  is also shown.

**Step 5. Calculate FoM.** Assume that  $W \sim \mathcal{N}(80 \text{ MHz}, (2 \text{ MHz})^2)$  ( $5\sigma = 10 \text{ MHz}$ ) and that

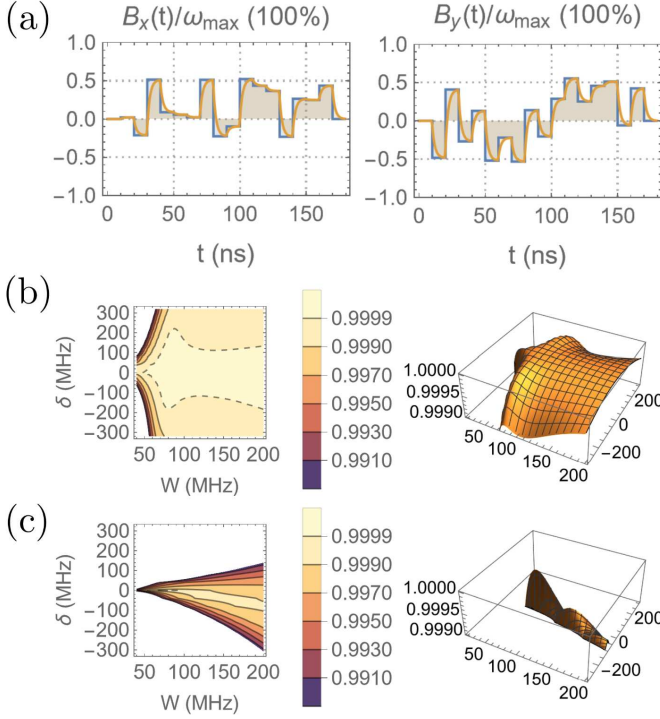


FIG. 4: (a) Control sequence for Hadamard gate that is robust to  $\tau_c$  and  $\delta$  variations. The blue and orange curves represent the relative amplitudes of  $B_x(t)$  and  $B_y(t)$  before and after distortion. (b) Contour and 3D landscape of fidelity for the robust sequence. (c) Same as (b) but for a non-robust sequence of the same  $T_{\text{seq}}$ .

$\delta \sim \mathcal{N}(0, (4 \text{ MHz})^2)$  ( $5\sigma = 20 \text{ MHz}$ ). The FoM of the robust and non-robust sequences are  $0.999995^{+0.000003}_{-0.000002}$  and  $0.99994^{+0.00004}_{-0.00003}$ .

### C. Robust control with nonlinear system

The dynamics of the control system are, in general, nonlinear. Here, we show an important example of a weak nonlinearity for a kinetic inductance.

Generally, the output field  $\vec{B}(t)$  and the input parameter  $\{a_k(t)\}$  are related through a state-space differential equation

$$\frac{d\vec{B}}{dt} = h(\vec{B}(t), \{a_k(t)\}, t; \{\mu_j\}), \quad (34)$$

where  $h$  is a nonlinear function. We can design control sequences robust to variations in  $\{\mu_j\}$  provided that the equation is not chaotic. As an example, consider the resonant circuit in Fig. 5. We design a Hadamard gate that is robust to small kinetic inductance. This method can be used to design robust sequences against variations in parameters in general nonlinear control systems.

Step 1. System and controls. Start with the same in-

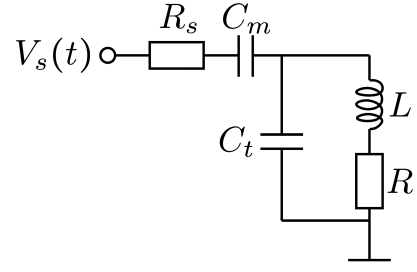


FIG. 5: A simple resonant circuit with  $R_s = 50 \Omega$ ,  $R = 0.01 \Omega$ ,  $C_m = 11 \text{ fF}$ ,  $C_t = 1.479 \text{ pF}$ , and  $L = 170 \text{ pH}$ . The resonance frequency is 10 GHz.

ternal and control Hamiltonians in Eqs. (29). The control field  $\vec{B}(t)$  can be obtained by solving the following differential equation in the rotating frame [57, 58]

$$\frac{dx}{dt} = A(x)x + \alpha(t)u, \quad (35)$$

where

$$\begin{aligned} x &= (\tilde{I}_L, \tilde{V}_{C_m}, \tilde{V}_{C_t})^T, \\ A(x) &= \begin{pmatrix} -\frac{R}{L} & 0 & \frac{1}{L} \\ 0 & \frac{-1}{R_L C_m} & \frac{1}{R_L C_m} \\ -\frac{1}{C_t} & \frac{-1}{R_L C_t} & \frac{1}{R_L C_t} \end{pmatrix} - i\omega_r \mathbb{1}, \\ u &= \left(0, \frac{1}{R_L C_m}, \frac{1}{R_L C_t}\right)^T, \end{aligned} \quad (36)$$

and the control parameters  $\{a_k(t)\}$  and the components of the output field  $\vec{B}(t)$  are

$$\begin{aligned} a_1(t) &= \kappa_i \text{Re}(\alpha(t)), \quad a_2(t) = \kappa_i \text{Im}(\alpha(t)), \\ B_x(t) &= \kappa_o \text{Re}(\tilde{I}_L)\omega_{\max}, \quad B_y(t) = \kappa_o \text{Im}(\tilde{I}_L)\omega_{\max}, \end{aligned} \quad (37)$$

where  $\omega_{\max} = 20 \text{ MHz}$ ,  $\kappa_i = 1 \text{ V}^{-1}$  and  $\kappa_o = 2 \text{ A}^{-1}$ .

In the presence of kinetic inductance [59], the inductance  $L$  depends on the current:

$$L = L_0(1 + \alpha_L |I_L|^2), \quad (38)$$

where  $\alpha_L$  is a constant, leading to nonlinear behavior in the circuit [59–61]. The model parameters are the electrical component parameters in the circuit where  $\alpha_L \sim \text{Unif}[-0.001, 0.001] \text{ A}^{-2}$ . Note,  $\alpha_L$  is typically positive, but we can still design around  $\alpha_L = 0$ . The solution is robust to  $\alpha_L$  that is either positive or negative. The error Hamiltonian  $\Delta H$  can be calculated by solving the differential equation of  $\partial x / \partial \alpha_L$ . The general method is provided in the Supplemental material.

Steps 2 and 3 are the same as the previous example.

Step 4. Robustness and optimization. Design for a fidelity of 0.9999 or higher. Fig. 6 shows robust and non-robust Hadamard gates. Their control landscapes are shown in Fig. 7.

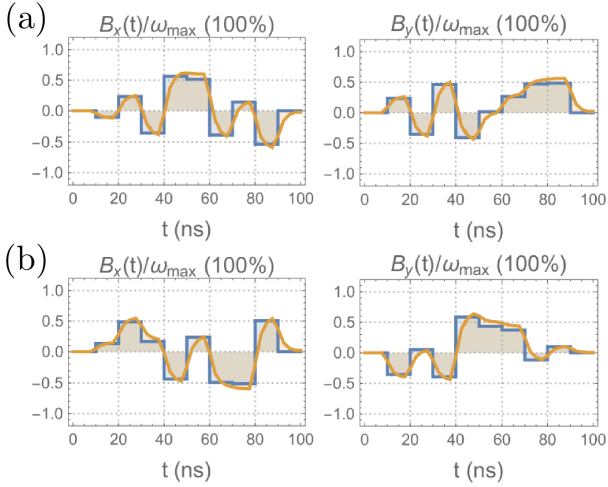


FIG. 6: The control parameters (blue) and the relative amplitudes of the  $x$  and  $y$  components of  $\vec{B}(t)$  at  $\alpha_L = 0$  for (a) a non-robust sequence and (b) a sequence robust to variations in  $\alpha_L$ .

Step 5. Calculate FoM. To simulate the FoM, we assume that  $\alpha_L$  obeys a half Gaussian distribution,  $\alpha_L \sim \mathcal{HN}(0, (0.0002 \text{ A}^{-2})^2)$  ( $5\sigma = 0.001 \text{ A}^{-2}$ ). The FoM of the robust and non-robust sequences are  $0.99991_{-0.00003}^{0.00008}$  and  $0.997_{-0.002}^{+0.003}$ .

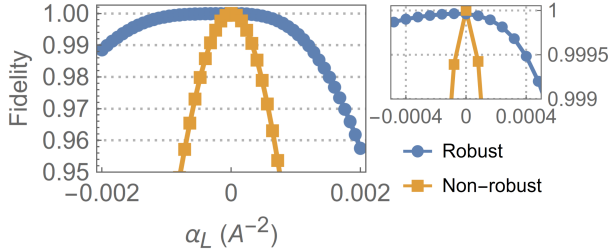


FIG. 7: Control landscapes of different sequences as a function of the nonlinear coefficient  $\alpha_L$ . The main panel shows the full fidelity profile; the smaller panel on the right displays a zoomed view around the high-fidelity region near  $\alpha_L = 0$ . Although the robustness extends to negative  $\alpha_L$ ,  $\alpha_L$  is typically positive.

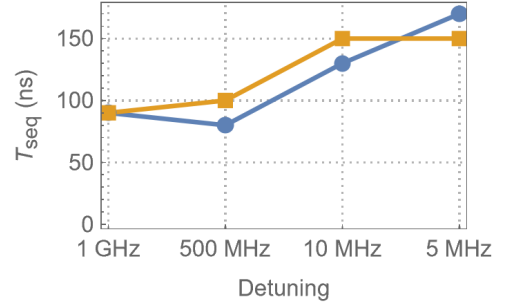
#### D. Two-qubit gates

The methods for designing robust two-qubit gates are the same as those discussed above. There are additional terms such as the leakage between controls on different qubits which can reduce the efficiency of a sequence. Additionally, different forms of qubit interactions can result in different efficiencies. Fig. 8 shows the minimal lengths of the sequences we found for a CNOT. We compare the efficiency of sequence design under Ising and Heisenberg

interactions, using the same interaction strength  $J$ :

$$\begin{aligned} H_{\text{Ising}} &= J\sigma_z \otimes \sigma_z, \\ H_{\text{Heisenberg}} &= J(\sigma_x \otimes \sigma_x + \sigma_y \otimes \sigma_y + \sigma_z \otimes \sigma_z)/\sqrt{3}. \end{aligned} \quad (39)$$

The minimal sequence length increases as the qubit detuning  $\Delta$  decreases (i.e., as leakage increases). The results also reveal efficiency differences arising from the form of the interaction. This indicates that even when controllability remains unchanged, different system modalities can impact the efficiency of sequence design.



—●— Ising interaction —■— Heisenberg interaction

FIG. 8: Minimal length of sequence for a CNOT gate with different detunings and interaction forms.

#### E. Simulating a Tunable Quantum Harmonic Oscillator

We show an example of simulating a truncated quantum harmonic oscillator (QHO) using two qubits. The Hamiltonian of a QHO is  $H_{\text{QHO}} = \hbar\Omega(\hat{N} + 1/2)$ . Using the code [62]

$$\begin{aligned} |n=0\rangle &= |00\rangle, \\ |n=1\rangle &= |01\rangle, \\ |n=2\rangle &= |11\rangle, \\ |n=3\rangle &= |10\rangle, \end{aligned} \quad (40)$$

an evolution under  $H_{\text{QHO}}$  can be simulated by implementing

$$U(T_{\text{seq}}) = \exp[i\{\sigma_z^2(1 + \sigma_z^1/2) - 2\}\Omega T_{\text{seq}}]. \quad (41)$$

With universal control over the two qubits, a solution to realize  $U(T_{\text{seq}})$  can be easily found using algorithms such as GRAPE [43, 63] or CRAB [64, 65]. We consider a different approach using Hamiltonian engineering that enables the direct control of the scaling of the simulated dynamics with an input parameter.

Step 1. System and controls. Assume that the bandwidth of the control system is very large and variations in control and model parameters are negligible. In the

rotating frame of the qubits, the control and internal Hamiltonians are

$$\begin{aligned}
 H_c(t) &= \omega_1^1(t) [\cos(\phi_1(t))\sigma_x^1 + \sin(\phi_1(t))\sigma_y^1] + \Delta\omega_1(t)\sigma_z^1 \\
 &\quad + \omega_1^2(t) [\cos(\phi_2(t))\sigma_x^2 + \sin(\phi_2(t))\sigma_y^2] + \Delta\omega_2(t)\sigma_z^2, \\
 H_{\text{int}} &= J(\sigma_x^1\sigma_x^2 + \sigma_y^1\sigma_y^2 + \sigma_z^1\sigma_z^2).
 \end{aligned} \tag{42}$$

The control parameters are  $\omega_i^j(t)$ ,  $\theta_i(t)$  and  $\Delta\omega_i$  for  $i = 1, 2$ .  $J = 1.4$  MHz,  $\Delta\omega \sim \text{Unif}[-1, 1]$  MHz and  $T_1 = 100$  ms.

Step 2. Objectives and partitioning of  $H_{\text{tot}}$ . Set  $\Delta\omega_1(t) \equiv \Delta\omega$  and  $\Delta\omega_2(t) \equiv 0$ , and define the primary and perturbative Hamiltonians as

$$\begin{aligned}
 H_{\text{pri}} &= \omega_1^1(t)(\cos(\phi_1(t))\sigma_x^1 + \sin(\phi_1(t))\sigma_y^1) \\
 &\quad + \omega_1^2(t)(\cos(\phi_2(t))\sigma_x^2 + \sin(\phi_2(t))\sigma_y^2) \\
 &\quad + J(\sigma_x^1\sigma_x^2 + \sigma_y^1\sigma_y^2 + \sigma_z^1\sigma_z^2), \\
 H_{\text{pert}} &= \Delta\omega\sigma_z^1.
 \end{aligned} \tag{43}$$

$H_{\text{pert}}$  depends on the offset  $\Delta\omega$  which can be adjusted at the start of each experiment to modify the rate of the dynamics. The objectives are  $U_{\text{pri}} = \mathbb{1}$  and  $H_{\text{target}} = s\Delta\omega(\sigma_z^2(1 + \sigma_z^1/2))$ .

Step 3. Controllability. Using Algorithm 1,  $\mathbf{g}_{\text{pri}}$  generates universal control on the two qubits. Thus,  $U_{\text{pri}}$  is achievable. Using Algorithm 2,  $\mathcal{C}(\mathbf{g}_{\text{pri}}, H_{\text{pert}})$  is fifteen-dimension and includes  $H_{\text{target}}$ . Using Algorithm 3, we find that the achievable range of  $s$  is  $[-0.6(2), 0.6(8)]$ . Since the scaling of  $H_{\text{target}}$  can be controlled by adjusting  $\Delta\omega$ , we design for  $s > 0.1$ .

Step 4. Robustness and optimization. Design for fidelity 0.9999 or higher. To achieve precision in the engineered effective Hamiltonian, we choose to minimize  $\bar{H}^{(1)}$ . Note, since  $H_{\text{int}}$  is included in  $H_{\text{pri}}$ ,  $\bar{H}^{(1)}$  cannot be removed by symmetrizing the sequence. Instead, the generic condition (Supplementary) for removing  $\bar{H}^{(1)}$  is used in the optimization. Fig. 9 shows an optimized sequence ( $T_{\text{seq}} = 120$  ns), the control landscape is shown on the left of Fig. 10. This sequence achieves a scaling factor of 0.221.

Step 5. Calculate FoM. Assume that  $\Delta\omega \sim \mathcal{N}(0, (200 \text{ kHz})^2)$ , the FoM of the sequence is  $0.999997^{+0.000006}_{-0.000005}$ .

As mentioned before, the sequence allows simulation of a tunable QHO whose frequency can be adjusted by directly changing  $\Delta\omega_1(t) \equiv \Delta\omega$ . the right-hand side of Fig. 10 shows the survival probability of  $(|n=1\rangle + |n=3\rangle)/\sqrt{2}$  under the sequence with different values of  $\Delta\omega$ .

## F. Sensing with a Scalable Spin Amplifier

Consider designing a scalable solution for realizing a spin amplifier for measuring the state of a qubit. The quantum system of the target qubit and the spin amplifier is initially prepared in the state  $|\phi_T\rangle \otimes |0_1 0_2 \dots 0_N\rangle$ .

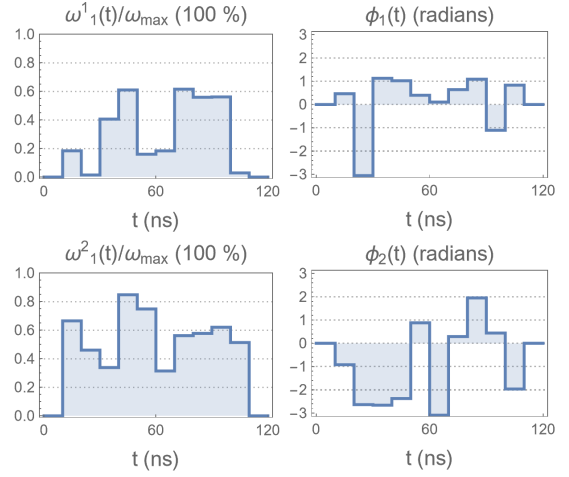


FIG. 9: Time-dependent control parameters of an optimized sequence that engineers a tunable QHO.

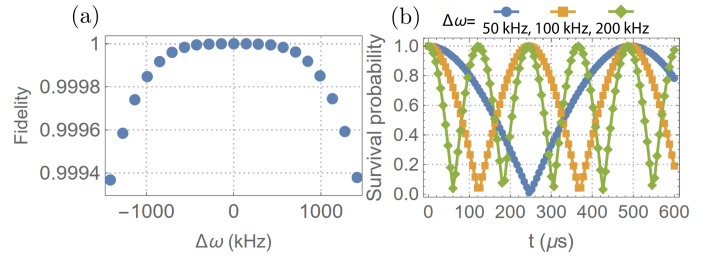


FIG. 10: (a) Control landscape of the sequence (Fig. 9) for simulating a QHO as a function of  $\Delta\omega$ . (b) Simulations of the evolution of the state  $(|n=1\rangle + |n=3\rangle)/\sqrt{2}$  under the sequence.

The goal is to design a sequence such that at the end of the sequence we can learn the state of the target qubit  $|\phi_T\rangle$  by measuring the collective magnetization  $M_z$  of qubits 1 to  $N$  in the spin amplifier.

A scalable solution can be obtained by engineering conditioned dynamics of the spin amplifier controlled by the state of the target qubit [66]. This can be achieved using internal interactions of the system and collective rotations of qubits in the spin amplifier.

We design a conditioned decoupling of the internal dynamics of the spin amplifier. Under the sequence, the internal interaction in the spin amplifier is decoupled if  $|\phi_T\rangle = |0\rangle$  and not decoupled if  $|\phi_T\rangle = |1\rangle$ . This interaction evolves the initial  $|00\dots 0\rangle$  into an entangled state with  $M_z \approx 0$  for large  $N$ . Therefore, after many applications of the sequence, measuring  $M_z$  reveals the target qubit state: if  $M_z \approx 1$  then  $|\phi_T\rangle = |0\rangle$ , if  $M_z \approx 0$  then  $|\phi_T\rangle = |1\rangle$ .

Step 1. System and controls. The internal and control

Hamiltonians are

$$H_c(t) = \omega_1(t) \left( \cos(\phi(t)) \sum_{i=1}^N \sigma_x^i + \sin(\phi(t)) \sum_{i=1}^N \sigma_y^i \right),$$

$$H_{\text{int}} = \sigma_z \otimes \sum_{i=1}^N \omega_i \sigma_z^i + \mathbb{1} \otimes \sum_{i<j}^N \omega_{ij} (2\sigma_z^i \otimes \sigma_z^j - \sigma_x^i \otimes \sigma_x^j - \sigma_y^i \otimes \sigma_y^j).$$
(44)

The control parameters are  $\omega(t)$  ( $\omega_{\text{max}} = 20$  MHz) and  $\phi(t)$ . The internal parameters are the coupling strengths:  $\omega_i \sim \text{Unif}[441, 459]$  kHz and  $\omega_{ij} \sim \text{Unif}[-22.5, 22.5]$  kHz.  $T_1 = 100$  ms.

Step 2. Objectives and partitioning of  $H_{\text{tot}}$ . Define the primary and perturbative Hamiltonians as

$$H_{\text{pri}}(t) = H_c(t) + \sigma_z \otimes \sum_{i=1}^N \omega_0 \sigma_z^i,$$

$$H_{\text{pert}}^1 = \sigma_z \otimes \sum_{i=1}^N (\omega_i - \omega_0) \sigma_z^i,$$

$$H_{\text{pert}}^2 = \mathbb{1} \otimes \sum_{i<j}^N \omega_{ij} (2\sigma_z^i \otimes \sigma_z^j - \sigma_x^i \otimes \sigma_x^j - \sigma_y^i \otimes \sigma_y^j),$$
(45)

where  $\omega_0 = 450$  kHz. The objectives are

$$U_{\text{pri}} = \mathbb{1},$$

$$H_{\text{target}}^2 = s\sqrt{2} \left[ |1\rangle\langle 1| \otimes \sum_{i<j}^N \omega_{ij} (2\sigma_z^i \otimes \sigma_z^j - \sigma_x^i \otimes \sigma_x^j - \sigma_y^i \otimes \sigma_y^j) \right].$$
(46)

Step 3. Controllability. To check the controllability, it is sufficient to consider two spins from the spin amplifier. Via Algorithm 1,  $\mathbf{g}_{\text{pri}}$  is three-dimensional and  $U_{\text{pri}} = \mathbb{1}$  is achievable. Using Algorithm 2,  $\mathcal{C}_2(\mathbf{g}_{\text{pri}}, H_{\text{pert}}^2)$  is ten-dimensional and includes  $H_{\text{target}}^2$ . Using Algorithm 3, we can find the achievable range of the scaling factor  $s$  (Table II). For comparison, Table II also lists some other achievable  $H_{\text{target}}^2$  and their ranges of scaling factors.

Step 4. Robustness and optimization. Design for a fidelity of 0.9999 or higher. Fig. 11 shows an optimized sequence ( $T_{\text{seq}} = 120$  ns). It achieves a scaling factor of  $s = 0.327$ . To obtain its control landscape, consider a

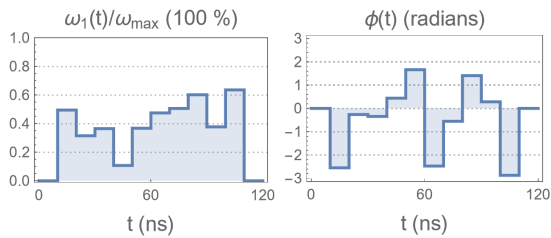


FIG. 11: Time-dependent control parameters of the sequence that achieves a scalable spin amplifier through engineering a conditioned decoupling.

spin amplifier of 6 qubits with the coupling strengths generated from  $\omega_i \sim \text{Unif}[450 - \delta\omega, 450 + \delta\omega]$  kHz and  $\omega_{ij} \sim \text{Unif}[-22.5, 22.5]$  kHz. The mean fidelity for different values of  $\delta\omega$  is plotted in Fig. 12.

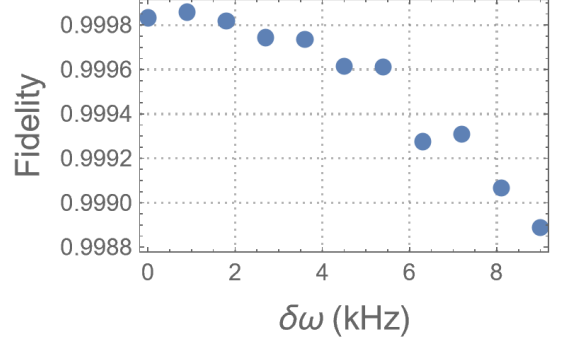


FIG. 12: Control landscape of the sequence in Fig. 11. The parameter  $\Delta\omega$  determines the width of the distribution of the coupling strength between the target qubit and the spin amplifier. The oscillations in fidelity arise from averaging over randomly sampled coupling strengths.

Step 5. Calculate FoM. To calculate the FoM of the sequence, use a spin amplifier of 6 qubits with the coupling strengths generated from  $\omega_i \sim \text{Unif}[441, 459]$  kHz and  $\omega_{ij} \sim \text{Unif}[-22.5, 22.5]$  kHz. The FoM, calculated as the average gate fidelity of the sequence, is  $0.9997_{-0.0001}^{+0.0001}$ .

To test the sequence, a simulation is conducted with the same spin amplifier used in the calculation of the FoM. The survival probabilities of the states

$$|\psi_{0/1}\rangle = |\phi_T = 0/1\rangle \otimes |00\dots 0\rangle$$
(47)

under the sequence are plotted in Fig. 13. The survival probability is proportional to  $M_z$  and can be used to learn the state  $|\phi_T\rangle$ . As can be seen from the result, after  $20 \mu\text{s}$ ,

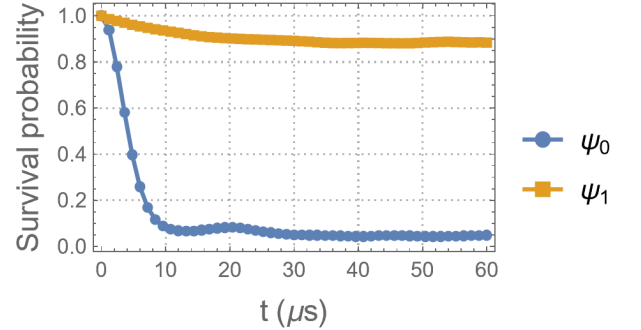


FIG. 13: Simulated survival probabilities of the states  $|\psi_{0/1}\rangle$  under the sequence in Fig. 11.

the survival probability of  $|\psi_0\rangle$  is above 0.8 while that of  $|\psi_1\rangle$  is below 0.1. So the states  $|\psi_{0/1}\rangle$  can be distinguished by measuring the magnetization of the spin amplifier, which is proportional to the survival probability.

TABLE II: Achievable ranges of scaling factors for different target effective Hamiltonians. They correspond to conditioned decoupling, double/zero quantum dynamics, and double/single quantum dynamics. Note, normalization constants have been omitted for simplicity.

Target Hamiltonian	Achievable range
$ 1\rangle\langle 1  \otimes (2\sigma_z \otimes \sigma_z - \sigma_x \otimes \sigma_x - \sigma_y \otimes \sigma_y)$	$[-0.353(5), 0.706(8)]$
$ 0\rangle\langle 0  \otimes (\sigma_x \otimes \sigma_x - \sigma_y \otimes \sigma_y) +  1\rangle\langle 1  \otimes (2\sigma_z \otimes \sigma_z - \sigma_x \otimes \sigma_x - \sigma_y \otimes \sigma_y)$	$[-0.408(2), 0.811(4)]$
$ 0\rangle\langle 0  \otimes (\sigma_x \otimes \sigma_y + \sigma_y \otimes \sigma_x) +  1\rangle\langle 1  \otimes (\sigma_x \otimes \sigma_z + \sigma_z \otimes \sigma_x)$	$[-0.576(4), 0.576(8)]$

In principle, one can include robustness by requiring  $H_{\text{target}}^1 = 0$  and including higher-order corrections [67]. In practice, however, we could not find a sequence that fulfills these requirements simultaneously while maintaining a high scaling factor without significantly increasing the length of the sequence. In turn, decreased scaling factor or fidelity of  $U_{\text{pri}}$  results in decreased FoM and inferior overall performance in sensing. This is because  $|H_{\text{pert}}^1| \ll |H_{\text{pert}}^2|$ , thus a larger scaling factor on  $H_{\text{pert}}^2$  is much more important. Also, large scaling factors are crucial when engineering nonzero effective Hamiltonians, as higher-order corrections are typically much smaller and less significant than the dominant low-order scaling.

## VI. DISCUSSION

Designing a control sequence is a complex task that depends on the control objective, the structure of both the internal and control Hamiltonians, and the limitations of classical control hardware. Here, we present a pseudocode framework (Algorithm 4) that connects these elements and guides the search for high-fidelity pulses. While our implementation is not unique, it offers the advantage of providing success metrics and a full error analysis.

The control sequence design process is compatible with a wide range of internal and control Hamiltonians and applies across the full range of quantum platforms. Typical control terms for two-level system qubit transitions (e.g., spin-based systems [68–70]) include Rabi strength, phase, and frequency offset of on-resonance or near-resonance drive. These controls act through microwave or laser fields and provide universal SU(2) control for each qubit. Similar control terms are used for effective qubits realized by selective driving of two energy levels in multi-level systems (e.g., superconducting qubits [71], trapped ions [72–74], and Rydberg atom arrays [75]), where leakage must be effectively managed [76, 77]. Other control building blocks include tuning of local potentials and tunneling rates in quantum dots [78, 79], setting amplitudes and phases of photonic modes in linear optics [80], and applying local modulations and mode couplings in cavity arrays [81]. These control terms define the control Hamiltonian  $H_c(t)$  and the time-dependent control parameters  $\{a_k(t)\}$ , while the electronic settings of the corresponding hardware specify the model parameters  $\{\mu_j\}$ . Uncertainties in  $\{\mu_j\}$  give the error Hamiltonians  $\{\Delta H_j\}$

(Set. IV and Step 1. (b)).

---

**Algorithm 4** Given the control parameters  $\{a_k(t)\}$ , the modal of the control system that maps  $\{a_k(t)\}$  to  $H_c(t)$  and distributions of  $\{\mu_j\}$  and  $\{\eta_{\text{int}}^i\}$ , the function FINDSEQUENCE takes the corresponding inputs and return a sequence  $\{a_k(t)\}$  that achieves the precision and robustness objectives.

---

```

1: function FINDSEQUENCE( $H_c(t, \bar{\mu})$ ,  $H_{\text{int}}$ ,  $H_{\text{pri}}(t)$ ,  $H_{\text{pert}}$ ,
    $U_{\text{target}}$ ,  $H_{\text{target}}$ ,  $s_{\text{target}}$ ,  $\mathcal{F}_{\text{target}}$ )
2:   for  $j = 1, \dots, J$  do
3:      $\Delta H_j \leftarrow \frac{\partial H_c}{\partial \mu_j}(\bar{\mu} = \bar{\mu}_0)$ 
4:   end for
5:   Determine a basis  $\{H_i\}$  of  $H_{\text{pri}}(t)$ 
6:    $\mathcal{B}(\mathbf{g}_{\text{pri}}) \leftarrow \text{FINDLIEALGEBRA}(\{H_i\}) \quad \triangleright$  Algorithm 1
7:   if  $U_{\text{target}} \in e^{\mathcal{B}(\mathbf{g}_{\text{pri}})}$  then
8:      $\mathcal{B}(\mathcal{C}) \leftarrow \text{FINDC}(\mathcal{B}(\mathbf{g}_{\text{pri}}), H_{\text{pert}}) \quad \triangleright$  Algorithm 2
9:     if  $H_{\text{target}} \in \mathcal{C}$  then
10:       $[s_-, s_+] \leftarrow \text{FINDSCALE}(\mathbf{g}_{\text{pri}}, H_{\text{pert}}) \triangleright$  Algorithm 3
11:     if  $s_{\text{target}} \in [s_-, s_+]$  then
12:       Determine robustness objectives (which
13:        $\Delta H_j$  to minimize) and higher-order corrections
14:       Use an optimizer to find  $\{a_k(t)\}$  and  $T_{\text{seq}}$ 
15:       that achieve the objectives ( $U_{\text{pri}}$ ,  $H_{\text{target}}$ , robustness and
16:       higher-order corrections)
17:     end if
18:     end if
19:     if If any of  $U_{\text{target}}$ ,  $H_{\text{target}}$  and  $s_{\text{target}}$  is unachievable
20:     then
21:       Modify the partitioning ( $H_{\text{pri}}$  and  $H_{\text{pert}}$ ) or include
22:       additional controls in  $H_c(t)$ . Restart the algorithm
23:     end if
24:      $\text{FoM} \leftarrow \mathcal{F}_{\text{ave}}(\{a_k(t)\}, U_{\text{target}} e^{-iH_{\text{target}}T_{\text{seq}}}) \quad \triangleright$  Eq. (19)
25:     Calculate the average CPTP map  $\bar{\Lambda} \quad \triangleright$  Eq. (18)
26:     if  $\text{FoM} \geq \mathcal{F}_{\text{target}}$  then
27:       return  $\{a_k(t)\}$ 
28:     else
29:       if  $\mathcal{R}(\bar{\Lambda})$  is small then  $\triangleright$  Eq. (28)
30:         Include higher-order robustness and correction
31:         terms
32:       else
33:         Increase target precision for  $U_{\text{pri}}$  and  $\bar{H}^{(0)}$  and
34:         include higher-order terms if  $H_{\text{target}} \neq 0$ 
35:       end if
36:       Update the objectives and restart the algorithm.
37:     end if
38: end function

```

---

Multi-qubit gates often rely on coupling between qubits, such as scalar or Fermi contact interactions, dipolar spin-spin coupling, coupling via shared resonators or direct capacitive or inductive elements in superconducting qubits, motional coupling in trapped ions, tunneling-enabled exchange interactions in quantum dots and neutral atoms, and effective interactions via measurement and post-selection in photonic systems. These couplings determine the internal Hamiltonians  $H_{\text{int}}$  and the internal parameters  $\{\eta_{\text{int}}^i\}$ . Typically, single-qubit effects like static offsets and inhomogeneities are also in  $H_{\text{int}}$  since they are not under direct control.

A partitioning of  $H_{\text{tot}}$  into  $H_{\text{pri}}$  and  $H_{\text{pert}}$  can then be chosen based on the control and internal Hamiltonians. The method described here identifies the set of achievable primary unitaries and perturbative effective Hamiltonians and designs control sequences that meet precision and robustness goals.

Note that partitioning is guided by three considerations: (1) optimizer efficiency, as different splits can change search difficulty; (2) controllability, since reachable targets depend on the partition; and (3) parameter tunability, as only parameters in  $H_{\text{pert}}$  appear in the engineered Hamiltonian. Parameters in  $H_{\text{pri}}$  are fixed once the sequence is found, while those in  $H_{\text{pert}}$  remain tunable. For high-fidelity implementations, fixed parameters are best placed in  $H_{\text{pri}}$ , as  $U_{\text{pri}}$  is generated by numerical integration and avoids errors due to truncation of the Magnus expansion.

While controllability tests determine whether a target is reachable, the time and quality of a resulting sequence depend on the choice of optimizer and partitioning. Although generalized simulated annealing [52] was used for the examples here, the method can be combined with various numerical optimization algorithms, such as Nelder-Mead [82, 83], nonlinear conjugate gradient [84], Powell's method [85], particle swarm [86], sequential convex programming [87], reinforcement learning [88], or differential evolution [89]. In general, global optimality is not achieved, and the optimizer will converge to a local solution.

If a sequence is hard to find, the partitioning of the total Hamiltonian can be adjusted. A practical strategy is to allow the optimizer to adaptively modify the weight of terms in  $H_{\text{pri}}$  and  $H_{\text{pert}}$ , provided controllability is preserved. This can lead to shorter and more easily discovered sequences.

The algorithm supports optimization for the largest possible scaling factor, which is key to achieving high efficiency. When designing a sequence for nonzero  $\bar{H}^{(0)}$ , achieving large scaling factors is typically more important than accounting for higher-order corrections. This is due to two reasons: first, higher-order terms typically scale as  $O(\|H_{\text{pert}}\|/\omega_{\text{mod}})^n$  so when the strength of the modulation  $\omega_{\text{mod}}$  is larger than  $\|H_{\text{pert}}\|$ ,  $\bar{H}^{(0)}$  dominates higher-order terms; and second, higher-order terms are modulated by  $\bar{H}^{(0)}$  due to a second averaging effect [90, 91].

Take  $\bar{H}^{(1)}$  as an example,

$$U(T_{\text{seq}}) \approx \exp[-i(s\bar{H}^{(0)} + \bar{H}^{(1)})T_{\text{seq}}]. \quad (48)$$

In the interaction frame of  $s\bar{H}^{(0)}$ ,  $\bar{H}^{(1)}$  becomes  $e^{is\bar{H}^{(0)}T_{\text{seq}}}\bar{H}^{(1)}e^{-is\bar{H}^{(0)}T_{\text{seq}}}$ . If  $[\bar{H}^{(0)}, \bar{H}^{(1)}] \neq 0$ ,  $\bar{H}^{(1)}$  is modulated by  $s\bar{H}^{(0)}$  and its average scales as  $1/s$  over repeated applications of the sequence. However, when  $s$  is small or  $[\bar{H}^{(0)}, \bar{H}^{(1)}] = 0$ , it is still important to account for  $\bar{H}^{(1)}$  and higher-order terms.

The method naturally includes parameter dispersions with moderate to long correlation times. Control landscapes (fidelity maps over internal and model parameters) provide insight into precision and robustness. A broad, flat high-fidelity region generally indicates greater robustness to parameter variations. Sequences can be designed for high fidelity across parameter distributions, with performance quantified by an average gate fidelity FoM. The computation of the FoM allows the inclusion of Markovian noise and relaxation processes, either via Lindbladian master equations or by composing with noise channels when they commute with the target unitary (e.g., depolarizing channels).

Finally, by outputting the average CPTP map  $\bar{\Lambda}$  or a corresponding Kraus representation, we gain diagnostic access to residual errors. The orthogonality  $\mathcal{R}(\bar{\Lambda})$  captures robustness, while its fidelity reflects both precision and robustness. These diagnostics help assess whether a sequence meets requirements or needs further refinement. Further diagnosis of possible error mechanisms can be achieved by expressing  $\bar{\Lambda}$  in its Kraus sum representation [92], which provides the set of possible errors that is important for the design of quantum error correction codes [93]. Future work will account for correlated environmental noise.

## VII. CONCLUSION

This work presents a general framework for precise and robust quantum control through effective Hamiltonian engineering which addresses two important issues: robustness to variations in parameters achieved by minimizing the effective Hamiltonian of the error Hamiltonian; and the benefit when designing a control sequence of identifying the subspace of the achievable zeroth-order average Hamiltonians. Generic conditions for removing higher-order corrections are also introduced. The framework is combined with numerical optimization to design optimized sequences.

The methods provided here represent a useful step toward the automated design of high-performance sequences for quantum control in different systems.

## ACKNOWLEDGMENTS

This work was supported by the Canadian Excellence Research Chairs (CERC) program, the Natural Sciences

and Engineering Research Council of Canada (NSERC) Discovery program, the Canada First Research Excellence Fund (CFREF), and the Innovation for Defence Excellence and Security (IDEaS) Program of the Canadian Department of National Defence.

- 
- [1] M. A. Nielsen and I. L. Chuang, *Quantum computation and quantum information* (Cambridge university press, 2010).
- [2] D. P. DiVincenzo, The physical implementation of quantum computation, *Fortschritte der Physik: Progress of Physics* **48**, 771 (2000).
- [3] J. Preskill, Reliable quantum computers, *Proceedings of the Royal Society of London. Series A: Mathematical, Physical and Engineering Sciences* **454**, 385 (1998).
- [4] S. J. Glaser, U. Boscain, T. Calarco, C. P. Koch, W. Köckenberger, R. Kosloff, I. Kuprov, B. Luy, S. Schirmer, T. Schulte-Herbrüggen, *et al.*, Training schrödinger’s cat: Quantum optimal control: Strategic report on current status, visions and goals for research in europe, *The European Physical Journal D* **69**, 1 (2015).
- [5] J. M. Chow, J. M. Gambetta, A. D. Corcoles, S. T. Merkel, J. A. Smolin, C. Rigetti, S. Poletto, G. A. Keefe, M. B. Rothwell, J. R. Rozen, *et al.*, Universal quantum gate set approaching fault-tolerant thresholds? with superconducting qubits, *Physical review letters* **109**, 060501 (2012).
- [6] M. A. Pravia, N. Boulant, J. Emerson, A. Farid, E. M. Fortunato, T. F. Havel, R. Martinez, and D. G. Cory, Robust control of quantum information, *The Journal of chemical physics* **119**, 9993 (2003).
- [7] P. Cappellaro, J. Hodges, T. Havel, and D. Cory, Principles of control for decoherence-free subsystems, *The Journal of chemical physics* **125** (2006).
- [8] C. P. Koch, Controlling open quantum systems: tools, achievements, and limitations, *Journal of Physics: Condensed Matter* **28**, 213001 (2016).
- [9] M. H. Goerz, D. M. Reich, and C. P. Koch, Optimal control theory for a unitary operation under dissipative evolution, *New Journal of Physics* **16**, 055012 (2014).
- [10] J. W. Britton, B. C. Sawyer, A. C. Keith, C.-C. J. Wang, J. K. Freericks, H. Uys, M. J. Biercuk, and J. J. Bollinger, Engineered two-dimensional ising interactions in a trapped-ion quantum simulator with hundreds of spins, *Nature* **484**, 489 (2012).
- [11] P. W. Shor, Scheme for reducing decoherence in quantum computer memory, *Physical review A* **52**, R2493 (1995).
- [12] U. Haeberlen and J. S. Waugh, Coherent averaging effects in magnetic resonance, *Physical Review* **175**, 453 (1968).
- [13] J. S. Waugh, L. M. Huber, and U. Haeberlen, Approach to high-resolution nmr in solids, *Physical Review Letters* **20**, 180 (1968).
- [14] P. Mansfield, Symmetrized pulse sequences in high resolution nmr in solids, *Journal of Physics C: Solid State Physics* **4**, 1444 (1971).
- [15] W.-K. Rhim, D. Elleman, and R. Vaughan, Analysis of multiple pulse nmr in solids, *The Journal of Chemical Physics* **59**, 3740 (1973).
- [16] D. Burum and W. Rhim, Analysis of multiple pulse nmr in solids. iii, *The Journal of Chemical Physics* **71**, 944 (1979).
- [17] K. Takegoshi and C. McDowell, A “magic echo” pulse sequence for the high-resolution nmr spectra of abundant spins in solids, *Chemical physics letters* **116**, 100 (1985).
- [18] D. Cory, J. Miller, and A. Garroway, Time-suspension multiple-pulse sequences: Applications to solid-state imaging, *Journal of Magnetic Resonance* (1969) **90**, 205 (1990).
- [19] D. Raleigh, M. Levitt, and R. G. Griffin, Rotational resonance in solid state nmr, *Chemical Physics Letters* **146**, 71 (1988).
- [20] M. Levitt, D. Raleigh, F. Creuzet, and R. Griffin, Theory and simulations of homonuclear spin pair systems in rotating solids, *The Journal of chemical physics* **92**, 6347 (1990).
- [21] W. Rose, H. Haas, A. Q. Chen, N. Jeon, L. J. Lauhon, D. G. Cory, and R. Budakian, High-resolution nanoscale solid-state nuclear magnetic resonance spectroscopy, *Physical Review X* **8**, 011030 (2018).
- [22] H. Haas, S. Tabatabaei, W. Rose, P. Sahafi, M. Piscitelli, A. Jordan, P. Priyadarsi, N. Singh, B. Yager, P. J. Poole, *et al.*, Nuclear magnetic resonance diffraction with subangstrom precision, *Proceedings of the National Academy of Sciences* **119**, e2209213119 (2022).
- [23] M. F. O’Keeffe, L. Horesh, J. F. Barry, D. A. Braje, and I. L. Chuang, Hamiltonian engineering with constrained optimization for quantum sensing and control, *New Journal of Physics* **21**, 023015 (2019).
- [24] F. Poggiali, P. Cappellaro, and N. Fabbri, Optimal control for one-qubit quantum sensing, *Physical Review X* **8**, 021059 (2018).
- [25] C. Tseng, S. Somaroo, Y. Sharf, E. Knill, R. Laflamme, T. F. Havel, and D. G. Cory, Quantum simulation of a three-body-interaction hamiltonian on an nmr quantum computer, *Physical Review A* **61**, 012302 (1999).
- [26] A. D. Bookatz, P. Wocjan, and L. Viola, Hamiltonian quantum simulation with bounded-strength controls, *New Journal of Physics* **16**, 045021 (2014).
- [27] K. X. Wei, C. Ramanathan, and P. Cappellaro, Exploring localization in nuclear spin chains, *Physical review letters* **120**, 070501 (2018).
- [28] M. Niknam, L. F. Santos, and D. G. Cory, Sensitivity of quantum information to environment perturbations measured with a nonlocal out-of-time-order correlation function, *Physical Review Research* **2**, 013200 (2020).
- [29] P. Peng, C. Yin, X. Huang, C. Ramanathan, and P. Cappellaro, Floquet prethermalization in dipolar spin chains, *Nature Physics* **17**, 444 (2021).
- [30] R. A. Jalabert and H. M. Pastawski, Environment-independent decoherence rate in classically chaotic systems, *Physical review letters* **86**, 2490 (2001).
- [31] A. M. Souza, G. A. Alvarez, and D. Suter, Robust dynamical decoupling for quantum computing and quantum memory, *Physical review letters* **106**, 240501 (2011).

- [32] Z. Tošner, T. Vosegaard, C. Kehlet, N. Khaneja, S. J. Glaser, and N. C. Nielsen, Optimal control in nmr spectroscopy: Numerical implementation in simpson, *Journal of Magnetic Resonance* **197**, 120 (2009).
- [33] L. Viola, E. Knill, and S. Lloyd, Dynamical decoupling of open quantum systems, *Physical Review Letters* **82**, 2417 (1999).
- [34] W. Zhang, N. Konstantinidis, V. Dobrovitski, B. Harmon, L. F. Santos, and L. Viola, Long-time electron spin storage via dynamical suppression of hyperfine-induced decoherence in a quantum dot, *Physical Review B—Condensed Matter and Materials Physics* **77**, 125336 (2008).
- [35] J. Choi, H. Zhou, H. S. Knowles, R. Landig, S. Choi, and M. D. Lukin, Robust dynamic hamiltonian engineering of many-body spin systems, *Physical Review X* **10**, 031002 (2020).
- [36] H. Zhou, L. S. Martin, M. Tyler, O. Makarova, N. Leitao, H. Park, and M. D. Lukin, Robust higher-order hamiltonian engineering for quantum sensing with strongly interacting systems, *Physical Review Letters* **131**, 220803 (2023).
- [37] M. Tyler, H. Zhou, L. S. Martin, N. Leitao, and M. D. Lukin, Higher-order methods for hamiltonian engineering pulse sequence design, *Physical Review A* **108**, 062602 (2023).
- [38] P. Peng, X. Huang, C. Yin, L. Joseph, C. Ramanathan, and P. Cappellaro, Deep reinforcement learning for quantum hamiltonian engineering, *Physical Review Applied* **18**, 024033 (2022).
- [39] Y. Baum, M. Amico, S. Howell, M. Hush, M. Liuzzi, P. Mundada, T. Merkh, A. R. Carvalho, and M. J. Biercuk, Experimental deep reinforcement learning for error-robust gate-set design on a superconducting quantum computer, *PRX Quantum* **2**, 040324 (2021).
- [40] E. M. Fortunato, M. A. Pravia, N. Boulant, G. Teklemariam, T. F. Havel, and D. G. Cory, Design of strongly modulating pulses to implement precise effective hamiltonians for quantum information processing, *The Journal of chemical physics* **116**, 7599 (2002).
- [41] H. Haas, D. Puzzuoli, F. Zhang, and D. G. Cory, Engineering effective hamiltonians, *New Journal of Physics* **21**, 103011 (2019).
- [42] G. H. Golub and C. F. Van Loan, *Matrix computations* (JHU press, 2013).
- [43] N. Khaneja, T. Reiss, C. Kehlet, T. Schulte-Herbrüggen, and S. J. Glaser, Optimal control of coupled spin dynamics: design of nmr pulse sequences by gradient ascent algorithms, *Journal of magnetic resonance* **172**, 296 (2005).
- [44] D. Puzzuoli, S. F. Lin, M. Malekakhlagh, E. Pritchett, B. Rosand, and C. J. Wood, Algorithms for perturbative analysis and simulation of quantum dynamics, *Journal of Computational Physics* **489**, 112262 (2023).
- [45] D. d’Alessandro, *Introduction to quantum control and dynamics* (Chapman and hall/CRC, 2021).
- [46] E. Magesan, D. Puzzuoli, C. E. Granade, and D. G. Cory, Modeling quantum noise for efficient testing of fault-tolerant circuits, *Physical Review A—Atomic, Molecular, and Optical Physics* **87**, 012324 (2013).
- [47] B. C. Gerstein and C. R. Dybowski, Transient techniques in nmr of solids: an introduction to theory and practice, (1985).
- [48] Y. S. Weinstein, T. F. Havel, J. Emerson, N. Boulant, M. Saraceno, S. Lloyd, and D. G. Cory, Quantum process tomography of the quantum fourier transform, *The Journal of chemical physics* **121**, 6117 (2004).
- [49] I. N. Hincks, D. G. Cory, and C. Ramanathan, Equivalent hamiltonians for state to state transfer in the case of partial quantum control, arXiv preprint arXiv:1111.0944 (2011).
- [50] F. Mezzadri, How to generate random matrices from the classical compact groups, arXiv preprint math-ph/0609050 (2006).
- [51] D. Hayes, S. T. Flammia, and M. J. Biercuk, Programmable quantum simulation by dynamic hamiltonian engineering, *New Journal of Physics* **16**, 083027 (2014).
- [52] C. Tsallis and D. A. Stariolo, Generalized simulated annealing, *Physica A: Statistical Mechanics and its Applications* **233**, 395 (1996).
- [53] C. P. Slichter, *Principles of magnetic resonance*, Vol. 1 (Springer Science & Business Media, 2013).
- [54] T. Schanze, An exact d-dimensional tsallis random number generator for generalized simulated annealing, *Computer physics communications* **175**, 708 (2006).
- [55] M. Mehring and J. S. Waugh, Phase transients in pulsed nmr spectrometers, *Review of Scientific Instruments* **43**, 649 (1972).
- [56] T. M. Barbara, J. F. Martin, and J. G. Wurl, Phase transients in nmr probe circuits, *Journal of Magnetic Resonance* (1969) **93**, 497 (1991).
- [57] I. Hincks, C. Granade, T. W. Borneman, and D. G. Cory, Controlling quantum devices with nonlinear hardware, *Physical Review Applied* **4**, 024012 (2015).
- [58] I. N. Hincks, C. E. Granade, T. W. Borneman, and D. G. Cory, Generating a control sequence for quantum control (2020), united States Patent.
- [59] S. A. Maas, *Nonlinear microwave and RF circuits* (Artech house, 2003).
- [60] H. Mohebbi, O. Benningshof, I. Taminiau, G. Miao, and D. Cory, Composite arrays of superconducting microstrip line resonators, *Journal of Applied Physics* **115** (2014).
- [61] T. Dahm and D. Scalapino, Theory of intermodulation in a superconducting microstrip resonator, *Journal of applied physics* **81**, 2002 (1997).
- [62] S. Somaroo, C. Tseng, T. Havel, R. Laflamme, and D. G. Cory, Quantum simulations on a quantum computer, *Physical review letters* **82**, 5381 (1999).
- [63] T. W. Borneman, M. D. Hürlimann, and D. G. Cory, Application of optimal control to cpmg refocusing pulse design, *Journal of Magnetic Resonance* **207**, 220 (2010).
- [64] T. Caneva, T. Calarco, and S. Montangero, Chopped random-basis quantum optimization, *Physical Review A—Atomic, Molecular, and Optical Physics* **84**, 022326 (2011).
- [65] M. M. Müller, R. S. Said, F. Jelezko, T. Calarco, and S. Montangero, One decade of quantum optimal control in the chopped random basis, *Reports on progress in physics* **85**, 076001 (2022).
- [66] P. Cappellaro, J. Emerson, N. Boulant, C. Ramanathan, S. Lloyd, and D. G. Cory, Entanglement assisted metrology, *Physical review letters* **94**, 020502 (2005).
- [67] To minimize the cross term between  $H_{\text{pert}}^1$  and  $H_{\text{pert}}^2$ , consider  $N = 2$ , the total Hamiltonian is

$$H_{\text{tot}}(t) = H_{\text{pri}}(t) + (\omega_1 - \omega_0)\sigma_z \otimes \sigma_z \otimes \mathbb{1} + (\omega_2 - \omega_0)\sigma_z \otimes \mathbb{1} \otimes \sigma_z + H_{\text{pert}}^2. \quad (49)$$

- Since both  $H_{\text{pri}}(t)$  and  $H_{\text{pert}}^2$  are symmetric with respect to a permutation of the two qubits in the spin amplifier, we only need to consider  $(\omega_1 - \omega_0)\sigma_z \otimes \sigma_z \otimes \mathbb{1}$  for leading-order robustness.
- [68] D. G. Cory, A. F. Fahmy, and T. F. Havel, Ensemble quantum computing by nmr spectroscopy, *Proceedings of the National Academy of Sciences* **94**, 1634 (1997).
- [69] T. W. Borneman and D. G. Cory, Bandwidth-limited control and ringdown suppression in high-q resonators, *Journal of Magnetic Resonance* **225**, 120 (2012).
- [70] G. Balasubramanian, I. Chan, R. Kolesov, M. Al-Hmoud, J. Tisler, C. Shin, C. Kim, A. Wojcik, P. R. Hemmer, A. Krueger, *et al.*, Nanoscale imaging magnetometry with diamond spins under ambient conditions, *Nature* **455**, 648 (2008).
- [71] P. Krantz, M. Kjaergaard, F. Yan, T. P. Orlando, S. Gustavsson, and W. D. Oliver, A quantum engineer's guide to superconducting qubits, *Applied physics reviews* **6** (2019).
- [72] M. J. Biercuk, H. Uys, J. W. Britton, A. P. VanDevender, and J. J. Bollinger, Ultrasensitive detection of force and displacement using trapped ions, *Nature nanotechnology* **5**, 646 (2010).
- [73] R. Blatt and C. F. Roos, Quantum simulations with trapped ions, *Nature Physics* **8**, 277 (2012).
- [74] H. Häffner, C. F. Roos, and R. Blatt, Quantum computing with trapped ions, *Physics reports* **469**, 155 (2008).
- [75] M. Saffman, T. G. Walker, and K. Mølmer, Quantum information with rydberg atoms, *Reviews of modern physics* **82**, 2313 (2010).
- [76] F. Motzoi, J. M. Gambetta, P. Rebentrost, and F. K. Wilhelm, Simple pulses for elimination of leakage in weakly nonlinear qubits, *Physical review letters* **103**, 110501 (2009).
- [77] J. M. Gambetta, F. Motzoi, S. Merkel, and F. K. Wilhelm, Analytic control methods for high-fidelity unitary operations in a weakly nonlinear oscillator, *Physical Review A—Atomic, Molecular, and Optical Physics* **83**, 012308 (2011).
- [78] D. Loss and D. P. DiVincenzo, Quantum computation with quantum dots, *Physical Review A* **57**, 120 (1998).
- [79] S. G. Philips, M. T. Madzik, S. V. Amitonov, S. L. de Snoo, M. Russ, N. Kalhor, C. Volk, W. I. Lawrie, D. Brousse, L. Trypuzen, *et al.*, Universal control of a six-qubit quantum processor in silicon, *Nature* **609**, 919 (2022).
- [80] E. Knill, R. Laflamme, and G. J. Milburn, A scheme for efficient quantum computation with linear optics, *nature* **409**, 46 (2001).
- [81] A. A. Houck, H. E. Türeci, and J. Koch, On-chip quantum simulation with superconducting circuits, *Nature Physics* **8**, 292 (2012).
- [82] J. A. Nelder and R. Mead, A simplex method for function minimization, *The computer journal* **7**, 308 (1965).
- [83] J. C. Lagarias, J. A. Reeds, M. H. Wright, and P. E. Wright, Convergence properties of the nelder–mead simplex method in low dimensions, *SIAM Journal on optimization* **9**, 112 (1998).
- [84] W. W. Hager and H. Zhang, A new conjugate gradient method with guaranteed descent and an efficient line search, *SIAM Journal on optimization* **16**, 170 (2005).
- [85] M. J. Powell, An efficient method for finding the minimum of a function of several variables without calculating derivatives, *The computer journal* **7**, 155 (1964).
- [86] J. Kennedy and R. Eberhart, Particle swarm optimization, in *Proceedings of ICNN'95-international conference on neural networks*, Vol. 4 (IEEE, 1995) pp. 1942–1948.
- [87] R. L. Kosut, M. D. Grace, and C. Brif, Robust control of quantum gates via sequential convex programming, *Physical Review A—Atomic, Molecular, and Optical Physics* **88**, 052326 (2013).
- [88] R. S. Sutton, A. G. Barto, *et al.*, *Reinforcement learning: An introduction*, Vol. 1 (MIT press Cambridge, 1998).
- [89] R. Storn and K. Price, Differential evolution—a simple and efficient heuristic for global optimization over continuous spaces, *Journal of global optimization* **11**, 341 (1997).
- [90] U. Haeberlen, *High Resolution NMR in solids selective averaging: supplement 1 advances in magnetic resonance*, Vol. 1 (Elsevier, 2012).
- [91] D. Cory, J. Miller, R. Turner, and A. Garroway, Multiple-pulse methods of 1h nmr imaging of solids: second-order averaging, *Molecular Physics* **70**, 331 (1990).
- [92] K. Kraus, General state changes in quantum theory, *Annals of Physics* **64**, 311 (1971).
- [93] E. Knill and R. Laflamme, Theory of quantum error-correcting codes, *Physical Review A* **55**, 900 (1997).

# Supplemental information: Engineering Precise and Robust Effective Hamiltonians

Jiahui Chen<sup>1,2\*</sup> and David Cory<sup>1,3</sup>

<sup>1</sup>*Institute for Quantum Computing, Waterloo, Ontario N2L 3G1, Canada*

<sup>2</sup>*Department of Physics, University of Waterloo, Waterloo, Ontario N2L 3G1, Canada*

<sup>3</sup>*Department of Chemistry, University of Waterloo, Waterloo, Ontario N2L 3G1, Canada*

(Dated: June 27, 2025)

## I. CALCULATING $\mathcal{C}(\mathfrak{g}_{\text{pri}}, H_{\text{pert}})$

Here, we prove a theorem that enables the calculation of  $\mathcal{C}(\mathfrak{g}_{\text{pri}}, H_{\text{pert}})$  using Algorithm 2 in the main text. Next, we discuss the representation for calculating  $\mathcal{C}(\mathfrak{g}_{\text{pri}}, H_{\text{pert}})$  and how to engineer multiple  $H_{\text{pert}}^w$  in parallel.

Define the adjoint map  $\text{ad}_A(B) = [A, B]$  for  $\forall$  (anti-)Hermitian operators  $A, B$  acting on the total Hilbert space  $\mathcal{H}$ .

**Theorem I.1.** *For a Hamiltonian  $H_{\text{pert}}$ , define*

$$\mathcal{C}(\mathfrak{g}_{\text{pri}}, H_{\text{pert}}) = \text{span}_{\mathbb{R}} \{ [g_1, \dots, [g_L, H_{\text{pert}}] \dots] | g_l \in \mathfrak{g}_{\text{pri}}, L \geq 0 \}, \quad (1)$$

and

$$\mathcal{O}(\mathfrak{g}_{\text{pri}}, H_{\text{pert}}) = \text{span}_{\mathbb{R}} \{ U_{\text{pri}}^\dagger(t) H_{\text{pert}} U_{\text{pri}}(t) dt | U_{\text{pri}}(t) \in e^{\mathfrak{g}_{\text{pri}}} \}. \quad (2)$$

Then  $\mathcal{C}(\mathfrak{g}_{\text{pri}}, H_{\text{pert}}) = \mathcal{O}(\mathfrak{g}_{\text{pri}}, H_{\text{pert}})$ .

*Proof.* Consider piecewise-continuous  $U(t)$ . For all  $U(t) \in e^{\mathfrak{g}_{\text{pri}}}$ , there exists  $g_t \in \mathfrak{g}_{\text{pri}}$ , such that  $U(t) = e^{g_t}$ . Therefore,  $e^{-g_t} H_{\text{pert}} e^{g_t} = e^{-\text{ad}_{g_t}}(H_{\text{pert}}) \in \mathcal{C}(\mathfrak{g}_{\text{pri}}, H_{\text{pert}})$  and  $\mathcal{O}(\mathfrak{g}_{\text{pri}}, H_{\text{pert}}) \subset \mathcal{C}(\mathfrak{g}_{\text{pri}}, H_{\text{pert}})$ .

Since  $\mathcal{H}$  is finite-dimensional, there exists  $m < |\mathcal{H}|^2 - 1$  such that  $\{H_{\text{pert}}, \text{ad}_g(H_{\text{pert}}), \dots, \text{ad}_g^{m+1}(H_{\text{pert}})\}$  is linearly dependent  $\forall g \in \mathfrak{g}_{\text{pri}}$ . Assume that  $\{H_{\text{pert}}, \text{ad}_g(H_{\text{pert}}), \dots, \text{ad}_g^m(H_{\text{pert}})\}$  is linearly independent and  $e^{g t_i} H_{\text{pert}} e^{-g t_i}$  is in

$$\text{span}_{\mathbb{R}} \{ H_{\text{pert}}, \text{ad}_g(H_{\text{pert}}), \dots, \text{ad}_g^m(H_{\text{pert}}) \}.$$

We can choose  $t_i$  for  $i = 1, \dots, m$  such that

$$[g, H_{\text{pert}}] \in \text{span}_{\mathbb{R}} \{ e^{g t_i} H_{\text{pert}} e^{-g t_i} | i = 1, \dots, m \}, \quad (3)$$

$\forall g_1, g_2 \in \mathfrak{g}_{\text{pri}}$ , we have

$$\begin{aligned} [g_2, [g_1, H_{\text{pert}}]] &= \sum_{j=1}^s a_j^2 e^{g_2 t'_j} [g_1, H_{\text{pert}}] e^{-g_2 t'_j} \\ &= \sum_{j=1}^s a_j^2 e^{g_2 t'_j} \left( \sum_{i=1}^m a_i^1 e^{g_1 t_i} H_{\text{pert}} e^{-g_1 t_i} \right) e^{-g_2 t'_j} \\ &= \sum_{j=1}^s \sum_{i=1}^m a_j^2 a_i^1 e^{g_{ij}} H_{\text{pert}} e^{-g_{ij}}, \end{aligned} \quad (4)$$

for some  $g_{ij} \in \mathfrak{g}_{\text{pri}}$ . The last equality is due to the Baker–Campbell–Hausdorff theorem. Therefore, by induction,  $[g_1, \dots, [g_L, H_{\text{pert}}]] \in \mathcal{O}(\mathfrak{g}_{\text{pri}}, H_{\text{pert}}) \forall g_1, \dots, g_L \in \mathfrak{g}_{\text{pri}}$ . Thus,  $\mathcal{C}(\mathfrak{g}_{\text{pri}}, H_{\text{pert}}) \subset \mathcal{O}(\mathfrak{g}_{\text{pri}}, H_{\text{pert}})$ .

Combining the result with the first part of the proof, we have  $\mathcal{C}(\mathfrak{g}_{\text{pri}}, H_{\text{pert}}) = \mathcal{O}(\mathfrak{g}_{\text{pri}}, H_{\text{pert}})$ .  $\square$

For time-dependent  $H_{\text{pert}}(t)$ , the space is define as  $\mathcal{C}(\mathfrak{g}_{\text{pri}}, \mathfrak{g}_{\text{pert}}) = [\mathfrak{g}_{\text{pri}}, \mathfrak{g}_{\text{pert}}]$ , where  $\mathfrak{g}_{\text{pert}}$  is the minimal Lie algebra containing  $H_{\text{pert}}(t)$ .

---

\* j562chen@uwaterloo.ca

It is convenient to choose a representation  $\phi$  of  $\mathbf{g}_{\text{pri}}$  and  $H_{\text{pert}}$  that is restricted to a subspace of  $\mathcal{H}$  to calculate  $\mathcal{C}(\mathbf{g}_{\text{pri}}, H_{\text{pert}})$ .  $\phi$  needs to preserve the structure of  $\mathcal{C}(\mathbf{g}_{\text{pri}}, H_{\text{pert}})$ , namely

$$[\phi(g), \phi(h_1)] = \phi(h_2) \iff [g, h_1] = h_2, \quad (5)$$

for all  $g \in \mathbf{g}_{\text{pri}}$  and  $h_1, h_2 \in \mathcal{C}(\mathbf{g}_{\text{pri}}, H_{\text{pert}})$ . The representation is bijective and unique up to isomorphism.

When a finite-dimensional representation does not exist, sometimes we can decompose  $H_{\text{pert}}$  into components and define a finite-dimensional representation for each component. A representative example is Eq. (3) from the main text where it is convenient to group the bilinear and linear terms into  $H_{\text{pert}}^1$  and  $H_{\text{pert}}^2$ , respectively. Another example is a qubit network with different clusters that are controlled independently (Fig. 1).

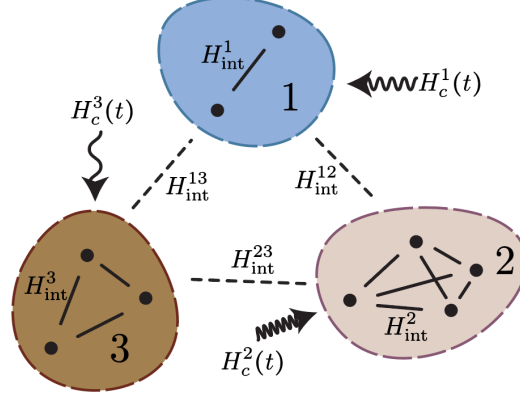


FIG. 1: A network of three clusters. Different clusters are controlled independently and have their own internal Hamiltonians.

## II. FINDING THE SET OF ACHIEVABLE $H_{\text{eff}}$

In this section, we first prove that the set of achievable  $\bar{H}^{(0)}$  is the convex hull of  $\{U_i^\dagger H_{\text{pert}} U_i\}$ ,  $U_i \in e^{\mathbf{g}_{\text{pri}}}$ . Then, the formal version of Algorithm 3 in the main text is given. Finally, the result is generalized to characterizing the range of achievable scaling factors when multiple  $H_{\text{pert}}^w$  are being engineered. It is convenient to use a vector representation of a Hamiltonian  $|H\rangle$  in  $\mathcal{C}(\mathbf{g}_{\text{pri}}, H_{\text{pert}})$  (Eqs. (24)), we have the following result.

**Theorem II.1.** *Define*

$$\mathcal{O}'(\mathbf{g}_{\text{pri}}, H_{\text{pert}}) = \left\{ \frac{1}{T_{\text{seq}}} \int_0^{T_{\text{seq}}} dt |U^\dagger(t) H_{\text{pert}} U(t)\rangle \middle| U(t) \in e^{\mathbf{g}_{\text{pri}}} \right\}, \quad (6)$$

$$\mathcal{Q}(\mathbf{g}_{\text{pri}}, H_{\text{pert}}) = \{ |U^\dagger H_{\text{pert}} U\rangle \mid U \in e^{\mathbf{g}_{\text{pri}}} \}. \quad (7)$$

Denote the convex hull of  $\mathcal{Q}(\mathbf{g}_{\text{pri}}, H_{\text{pert}})$  as  $\bar{\mathcal{Q}}(\mathbf{g}_{\text{pri}}, H_{\text{pert}})$ . Assume that any  $U \in e^{\mathbf{g}_{\text{pri}}}$  can be implemented in a time  $t_p$  much shorter than  $1/\|H_{\text{pert}}\|$ , then  $\mathcal{O}'(\mathbf{g}_{\text{pri}}, H_{\text{pert}}) = \bar{\mathcal{Q}}(\mathbf{g}_{\text{pri}}, H_{\text{pert}})$ .

*Proof.* An element from  $\bar{\mathcal{Q}}(\mathbf{g}_{\text{pri}}, |H_{\text{pert}}\rangle\rangle)$  takes the form  $\sum_{i=1}^M p_i |U_i^\dagger H_{\text{pert}} U_i\rangle$  for a positive integer  $M$  and probabilities  $\{p_i\}$ . Let

$$g \left( T_{\text{seq}} \sum_{j=1}^{i-1} p_j + t \right) = \begin{cases} \frac{g_i}{t_p} & t \in [0, t_p) \\ 0 & t \in [t_p, p_i T_{\text{seq}} - t_p) \\ \frac{-g_i}{t_p} & t \in [p_i T_{\text{seq}} - t_p, p_i T_{\text{seq}}] \end{cases}, \quad (8)$$

for  $i = 1, 2, \dots, M$ . Then

$$\lim_{t_p \rightarrow 0^+} \frac{1}{T_{\text{seq}}} \int_0^{T_{\text{seq}}} |U^\dagger(t) H_{\text{pert}} U(t)\rangle dt = \sum_{i=1}^M p_i |e^{-g_i} H_{\text{pert}} e^{g_i}\rangle. \quad (9)$$

Therefore,  $\bar{\mathcal{Q}}(\mathbf{g}_{\text{pri}}, H_{\text{pert}}) \subset \mathcal{O}'(\mathbf{g}_{\text{pri}}, H_{\text{pert}})$ . For all  $U(t) \in e^{\mathbf{g}_{\text{pri}}}$ ,

$$\begin{aligned} & \frac{1}{T_{\text{seq}}} \int_0^{T_{\text{seq}}} |U^\dagger(t) H_{\text{pert}} U(t)\rangle\rangle dt \\ &= \lim_{N \rightarrow \infty} \frac{1}{N} \sum_{i=1}^N \left| U^\dagger \left( \frac{i T_{\text{seq}}}{N} \right) H_{\text{pert}} U \left( \frac{i T_{\text{seq}}}{N} \right) \right\rangle\rangle \in \bar{\mathcal{Q}}(\mathbf{g}_{\text{pri}}, H_{\text{pert}}). \end{aligned} \quad (10)$$

The limit is valid if  $t_p \ll 1/\|H_{\text{pert}}\|$ . Thus,  $\mathcal{O}'(\mathbf{g}_{\text{pri}}, H_{\text{pert}}) \subset \bar{\mathcal{Q}}(\mathbf{g}_{\text{pri}}, H_{\text{pert}})$ . Therefore,  $\mathcal{O}'(\mathbf{g}_{\text{pri}}, H_{\text{pert}}) = \bar{\mathcal{Q}}(\mathbf{g}_{\text{pri}}, H_{\text{pert}})$ .  $\square$

If one can implement

$$\mathcal{T} \exp \left( -i \int_0^t H_{\text{tot}}(t') dt' \right) = \exp(-i H_{\text{pert}} t) U_t, \quad (11)$$

for all  $t > 0$  and some  $U_t \in e^{\mathbf{g}_{\text{pri}}}$ , e.g., when  $H_{\text{pri}}(t) = H_c(t) + p H_{\text{int}}$  and  $H_{\text{pert}} = (1-p) H_{\text{int}}$ , and  $H_{\text{pri}}(t) = H_c(t)$  and  $H_{\text{pert}}(t) = \epsilon H_c(t)$ , the condition  $t_p \ll 1/\|H_{\text{pert}}\|$  is unnecessary. Finite  $t_p$ , however, may limit the efficiency of a sequence.

Assuming that  $H_{\text{pert}}$  is normalized, for any normalized  $H_{\text{target}} \in \mathcal{C}$ , if there exists a sequence  $\{a_k(t)\}$  so that  $\bar{H}^{(0)}(T_{\text{seq}}) = s H_{\text{target}}$  for a real number  $s$  (or equivalently,  $s H_{\text{target}} \in \bar{\mathcal{Q}}(\mathbf{g}_{\text{pri}}, H_{\text{pert}})$ ), then  $s$  is an achievable scaling factor for  $H_{\text{target}}$ .  $\bar{\mathcal{Q}}(\mathbf{g}_{\text{pri}}, H_{\text{pert}})$  can be approximated using random unitaries  $\{u_j\}$ :

$$\bar{\mathcal{Q}}(\mathbf{g}_{\text{pri}}, H_{\text{pert}}) \approx \left\{ \sum_{j=1}^J x_j |u_j^\dagger H_{\text{pert}} u_j\rangle\rangle \left| \sum_{j=1}^J x_j = 1, x_j \geq 0, 1 \leq j \leq J \right. \right\}. \quad (12)$$

Choose a matrix  $T$  such that  $T|H_{\text{target}}\rangle\rangle = (1, 0, 0, \dots, 0)$  and define a set of vertices  $\{\bar{v}^j = T|u_j^\dagger H_{\text{pert}} u_j\rangle\rangle\}$ , the range of achievable scaling factors,  $[s_-, s_+]$ , can be found by solving the following linear programs

$$\begin{aligned} \text{LP}_\pm : & \text{Find a vector } \bar{x} \\ & \text{that maximizes } s_\pm = \bar{c}_\pm \cdot \bar{x} \text{ with } \bar{c}_\pm = (\pm 1, 0, \dots, 0) \\ & \text{subject to } \sum_i x_i = 1, -1 \leq \sum_i v_1^i x_i \leq 1 \\ & \text{and } \sum_i v_k^i x_i = 0, k = 2, 3, \dots \\ & \text{and } \bar{x} \geq 0 \end{aligned} \quad (13)$$

$H_{\text{target}}$  is not achievable if the constraint is infeasible (Fig. 2). The procedure is summarized as the following algorithm.

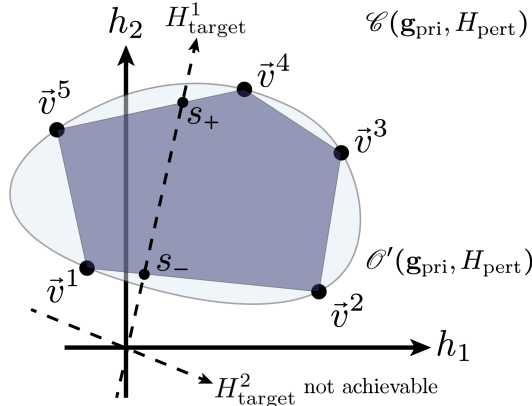


FIG. 2: Schematic for finding achievable scaling factors. The set of achievable zeroth-order average Hamiltonians  $\mathcal{O}'(\mathbf{g}_{\text{pri}}, H_{\text{pert}})$  (light blue area) is a convex set in  $\mathcal{C}(\mathbf{g}_{\text{pri}}, H_{\text{pert}})$  (spanned by  $h_1$  and  $h_2$ ). The convex set is approximated by the polygon (dark blue area) formed by  $\{\bar{v}_i = |u_i^\dagger H_{\text{pert}} u_i\rangle\rangle\}$ . The achievable scaling factors for  $H_{\text{target}}$  can then be found via linear programming.

**Algorithm 1** Algorithm for finding achievable scaling factors. The function FINDSCALE takes a basis of the primary Lie algebra  $\mathcal{B}(\mathfrak{g}_{\text{pri}})$ , a perturbative Hamiltonian  $H_{\text{pert}}$  and a target effective Hamiltonian  $H_{\text{target}}$  and returns either False when  $H_{\text{target}}$  is not achievable or the range of achievable scaling factors  $[s_-, s_+]$ .

---

```

1: function FINDSCALE( $\mathfrak{g}_{\text{pri}}, H_{\text{int}}, H_{\text{pert}}$ )
2:   Calculate  $\mathcal{B}(\mathcal{E})$ 
3:   find  $T$  such that  $T|H_{\text{target}}\rangle\rangle = (1, 0, \dots, 0)$ 
4:   for  $j = 1, \dots, J$  do
5:     Sample  $u_j \in e^{\mathfrak{g}_{\text{pri}}}$ 
6:      $\bar{v}^j \leftarrow T|u_j^\dagger H_{\text{pert}} u_j\rangle\rangle$ 
7:   end for
8:   Solve the linear programs LP+ and LP-
9:   if no solution exists then
10:    return False
11:  else
12:    return  $[s_-, s_+]$ 
13:  end if
14: end function

```

---

When

$$H_{\text{pert}} = \sum_{w=1}^W H_{\text{pert}}^w, \quad (14)$$

the condition for parallel effective Hamiltonian engineering is

$$\bigoplus_{w=1}^W |\bar{H}^{(0)w}\rangle\rangle_w = \bigoplus_{w=1}^W |H_{\text{target}}^w\rangle\rangle_w \equiv |H_{\text{target}}\rangle\rangle_{\text{total}}, \quad (15)$$

where  $|\cdot\rangle\rangle_w$  is the representation in  $\mathcal{C}_w(\mathfrak{g}_{\text{pri}}, H_{\text{pert}}^w)$ . We have

**Theorem II.2.** *Define*

$$\begin{aligned} \mathcal{O}'(\mathfrak{g}_{\text{pri}}, \{H_{\text{pert}}^w\}) &= \left\{ \frac{1}{T_{\text{seq}}} \int_0^{T_{\text{seq}}} dt \bigoplus_{w=1}^W |U_{\text{pri}}^\dagger(t) H_{\text{pert}}^w U_{\text{pri}}(t)\rangle\rangle_w \left| U_{\text{pri}}(t) \in e^{\mathfrak{g}_{\text{pri}}} \right. \right\}, \\ \mathcal{Q}(\mathfrak{g}_{\text{pri}}, \{H_{\text{pert}}^w\}) &= \left\{ \bigoplus_{w=1}^W |U_{\text{pri}}^\dagger H_{\text{pert}}^w U_{\text{pri}}\rangle\rangle_w \left| U_{\text{pri}} \in e^{\mathfrak{g}_{\text{pri}}} \right. \right\}. \end{aligned} \quad (16)$$

Then  $\mathcal{O}'(\mathfrak{g}_{\text{pri}}, \{H_{\text{pert}}^w\}) = \bar{\mathcal{Q}}(\mathfrak{g}_{\text{pri}}, \{H_{\text{pert}}^w\})$ .

Find  $T$  such that  $T|H_{\text{target}}\rangle\rangle_{\text{total}} \propto (1, 0, \dots, 0)$ , the vertices of the polygon are

$$\bar{v}^j = T \bigoplus_{w=1}^W |u_j^\dagger H_{\text{pert}}^w u_j\rangle\rangle_w. \quad (17)$$

**Corollary II.1.**  $\mathcal{O}'(\mathfrak{g}_{\text{pri}}, \{H_{\text{pert}}^w\}_{w=1}^W |H^{(0)1} = 0) = \mathcal{O}'(\mathfrak{g}_{\text{pri}}, \{H_{\text{pert}}^w\}_{w=2}^W)$ .

Namely, decoupling of any part of  $H_{\text{pert}}$  does not affect the controllability of others.

### III. GENERATING RANDOM UNITARIES FOR CONTROLLABILITY TEST

Here, we present algorithms for sampling random unitaries from  $e^{\mathfrak{g}_{\text{pri}}}$ . For standard groups such as the unitary groups, Haar random samples can be generated using the QR decomposition [1].

---

**Algorithm 2** Algorithm for generating random unitaries based on QR decomposition.

---

```

1: function RANDOMUQR( $n$ )
2:   generate two random real  $n \times n$  matrices  $r_1$  and  $r_2$  whose elements are sampled from  $\mathcal{N}(0, 1)$ 
3:    $z \leftarrow (r_1 + ir_2)/\sqrt{2}$ 
4:   use QR decomposition to decompose  $z$  into  $z = QR$  where  $Q$  is unitary and  $R$  is upper-triangle
5:   take the signs of the diagonal of  $R$  and form a diagonal matrix  $\Lambda$ 
6:   return  $Q\Lambda$ 
7: end function

```

---

For non-standard Lie algebras, we generate random unitaries from  $e^{\mathfrak{g}_{\text{pri}}}$  using a simple random walk algorithm [2].

---

**Algorithm 3** Algorithm for generating random unitaries using random walk.

---

```

1: function RANDOMULIE( $\mathcal{B}(\mathfrak{g}_{\text{pri}})$ )
2:    $g \leftarrow 0$ 
3:   for  $h \in \mathcal{B}(\mathfrak{g}_{\text{pri}})$  do
4:     sample  $p$  from  $\mathcal{N}(0, 1)$ 
5:      $g \leftarrow g + ph$ 
6:   end for
7:   return  $e^g$ 
8: end function
9: function RANDOMWALKU( $\mathcal{B}(\mathfrak{g}_{\text{pri}}), n_{\text{burn}}, n_{\text{thin}}, n_{\text{sample}}$ )
10:   $x \leftarrow \mathbb{1}$ 
11:  for  $1 \leq i_{\text{burn}} \leq n_{\text{burn}}$  do
12:     $x \leftarrow \text{RANDOMULIE}(\mathcal{B}(\mathfrak{g}_{\text{pri}})) \cdot x$ 
13:  end for
14:   $l_{\text{sample}} \leftarrow \{\}$ 
15:  for  $1 \leq i_{\text{sample}} \leq n_{\text{sample}}$  do
16:    for  $1 \leq i_{\text{thin}} \leq n_{\text{thin}}$  do
17:       $x \leftarrow \text{RANDOMULIE}(\mathcal{B}(\mathfrak{g}_{\text{pri}})) \cdot x$ 
18:    end for
19:    append  $x$  to  $l_{\text{sample}}$ 
20:  end for
21:  return  $l_{\text{sample}}$ 
22: end function

```

---

The convergence of the algorithm can be checked using, e.g., the coupling method. Alternatively, one can check the volume of the simulated  $\bar{\mathcal{Q}}$ . Fig. 3 shows the volume of the simulated  $\bar{\mathcal{Q}}$  of secular dipoler interaction under the collective control of the qubits. The volume is calculated using the quick hull algorithm [3, 4].

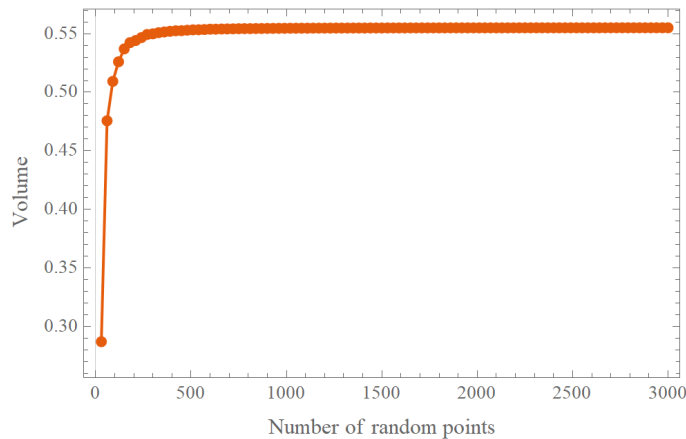


FIG. 3: Volume of the simulated  $\bar{\mathcal{Q}}$  as a function of the number of samples. It saturates after around 500 samples.

### A. Discretization of $\vec{B}(t)$ for integration

Here, we briefly describe the discretization of  $\vec{B}(t)$  for numerical integration. Note, this is required during pulse finding, but not when calculating the performance of a sequence. The control parameters  $a_k(t)$  are typically piecewise-constant:

$$a_{k,p} = a_k[(p-1/2)dt], \quad (18)$$

for  $p = 1, \dots, P$ . Here, an equal step length  $dt$  is assumed for the discretization for simplicity. Denote components of  $\vec{B}(t)$  in rotation frames of the qubits by  $\{b_k(t)\}$ , they can be discretized into  $Q$  steps (Fig. 4) and the value at the  $q$ th step  $b_{k,q}$  is approximated by the value of  $b_k(t)$  at the middle of the step

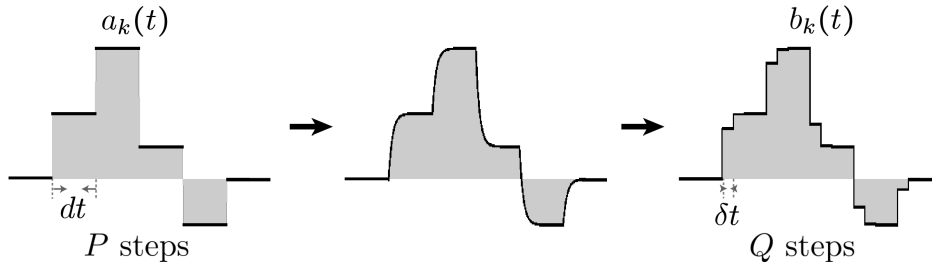


FIG. 4: Illustration of the discretization of output field parameters. The control parameters  $\{a_k(t)\}$  are mapped to  $\vec{B}(t)$  through the model of the control system. Then the continuous field  $\vec{B}(t)$  is discretized into  $Q$  steps for integration.

$$b_{k,q} = b_k[(q-1/2)\delta t], \quad (19)$$

so that  $Pdt = Q\delta t = T_{\text{seq}}$ .  $Q$  should be large enough in order to accurately represent  $\vec{B}(t)$ . The approximation (Eq. (19)) is reasonable when the time dependence of  $b_k(t)$  is much slower compared to  $1/\delta t$ . When the assumption does not hold, a better approximation is given by

$$b_{k,q} = \frac{1}{\delta t} \int_{(q-1)\delta t}^{q\delta t} b_k(t) dt. \quad (20)$$

The discretization enables straightforward calculation of the  $\mathcal{C}$ -integrals (defined below) by first computing them for each step and then composing them using a chain rule.

## IV. CALCULATING $\mathcal{C}$ -INTEGRALS FOR SHAPED PULSE

In this section, we show how to calculate the time-ordered integrals ( $\mathcal{C}$ -integrals)

$$\bar{c}_{i_1 \dots i_r}(T_{\text{seq}}) = \int_0^{T_{\text{seq}}} dt_1 \dots \int_0^{t_{r-1}} dt_r c_{i_1}(t_1) \dots c_{i_r}(t_r). \quad (21)$$

The  $\mathcal{C}$ -integrals are used for achieving robustness and accounting for higher-order corrections. First, we need to represent the toggling-frame Hamiltonian and the primary unitaries in  $\mathcal{C}(\mathbf{g}_{\text{pri}}, H_{\text{pert}})$ . Given an orthonormal basis of  $\mathcal{C}(\mathbf{g}_{\text{pri}}, H_{\text{pert}})$

$$\mathcal{B}(\mathcal{C}) = \{h_1, \dots, h_{|\mathcal{C}|}\}, \quad (22)$$

where  $|\mathcal{C}|$  is the dimension of  $\mathcal{C}(\mathbf{g}_{\text{pri}}, H_{\text{pert}})$ , for a Hamiltonian  $H$ , a unitary propagator  $U$  and a generator  $g$  of the unitary  $U = e^g$  acting on  $\mathcal{C}$ , their representations are denoted by  $|H\rangle$ ,  $\mathcal{D}(U)$  and  $\mathcal{D}(\text{ad}_g)$  respectively. They obey

$$|UHU^\dagger\rangle = \mathcal{D}(U)|H\rangle, \quad \mathcal{D}(e^g) = e^{\mathcal{D}(\text{ad}_g)}, \quad (23)$$

and can be calculated as

$$|H\rangle\rangle = \begin{pmatrix} \text{Tr}(Hh_1^\dagger) \\ \vdots \\ \text{Tr}(Hh_{|\mathcal{C}|}^\dagger) \end{pmatrix}, \quad \mathcal{D}(U) = \begin{pmatrix} \langle\langle h_1|Uh_1U^\dagger\rangle\rangle & \cdots & \langle\langle h_1|Uh_{|\mathcal{C}|}U^\dagger\rangle\rangle \\ \vdots & \ddots & \vdots \\ \langle\langle h_{|\mathcal{C}|}|Uh_1U^\dagger\rangle\rangle & \cdots & \langle\langle h_{|\mathcal{C}|}|Uh_{|\mathcal{C}|}U^\dagger\rangle\rangle \end{pmatrix}, \quad \mathcal{D}(\text{ad}_g) = \begin{pmatrix} \langle\langle h_1|[g, h_1]\rangle\rangle & \cdots & \langle\langle h_1|[g, h_{|\mathcal{C}|}]\rangle\rangle \\ \vdots & \ddots & \vdots \\ \langle\langle h_{|\mathcal{C}|}|[g, h_1]\rangle\rangle & \cdots & \langle\langle h_{|\mathcal{C}|}|[g, h_{|\mathcal{C}|}]\rangle\rangle \end{pmatrix}, \quad (24)$$

where  $\langle\langle \cdot | \star \rangle\rangle = \text{Tr}(\star \cdot^\dagger)$ .

Define

$$\vec{c}^{(r-1)} = (\bar{c}_{11\dots 1}, \bar{c}_{11\dots 2}, \dots, \bar{c}_{|\mathcal{C}||\mathcal{C}|\dots|\mathcal{C}|}), \quad (25)$$

then

$$\vec{c}^{(r-1)} = \int_0^{T_{\text{seq}}} dt_1 \cdots \int_0^{t_{r-1}} dt_r \mathcal{D}(U_{\text{pri}}^\dagger)(t_1) \otimes \cdots \otimes \mathcal{D}(U_{\text{pri}}^\dagger)(t_r) |H_{\text{pert}}(t_1)\rangle\rangle \otimes \cdots \otimes |H_{\text{pert}}(t_r)\rangle\rangle. \quad (26)$$

The discretization of  $\{b_k(t)\}$  is chosen to be fine enough so that during each step both  $H_{\text{pri}}(t)$  and  $H_{\text{pert}}(t)$  can be approximately viewed as constant. Denote their discretized versions corresponding to  $\{b_{k,q}\}$  by

$$\begin{aligned} \vec{H}_{\text{pri}} &= (H_{\text{pri}}^1, H_{\text{pri}}^2, \dots, H_{\text{pri}}^Q), \\ \vec{H}_{\text{pert}} &= (H_{\text{pert}}^1, H_{\text{pert}}^2, \dots, H_{\text{pert}}^Q). \end{aligned} \quad (27)$$

A recipe for calculating the  $\mathcal{C}$ -integrals for any sequence requires two ingredients: (1) Their calculation for a square pulse. (2) A chain rule of the  $\mathcal{C}$ -integrals that allows to calculate those of a sequence given the  $\mathcal{C}$ -integrals of the components of the sequence.

### A. $\mathcal{C}$ -integrals of a square pulse

During the  $q$ th step,  $H_{\text{pri}}(t) = H_{\text{pri}}^q$  and  $H_{\text{pert}}(t) = H_{\text{pert}}^q$ , so the  $\mathcal{C}$ -integrals become

$$\vec{c}^{(r-1)} = \int_0^{T_{\text{seq}}} dt_1 \cdots \int_0^{t_{r-1}} dt_r \exp(-i\mathcal{D}(\text{ad}_{H_{\text{pri}}^q})t_1) \otimes \cdots \otimes \exp(-i\mathcal{D}(\text{ad}_{H_{\text{pri}}^q})t_r) |H_{\text{pert}}^q\rangle\rangle^{\otimes r}. \quad (28)$$

Let  $\mathcal{D}(\text{ad}_{H_{\text{pri}}^q}) = TDT^\dagger$  where  $D$  is diagonal and  $T$  is a unitary matrix, the integral becomes

$$\vec{c}^{(r-1)} = T^{\otimes r} \left( I(\lambda_1, \lambda_1, \dots, \lambda_1), I(\lambda_1, \lambda_1, \dots, \lambda_2), \dots, I(\lambda_{|\mathcal{C}|}, \lambda_{|\mathcal{C}|}, \dots, \lambda_{|\mathcal{C}|}) \right)^T T^{\dagger \otimes r} |H_{\text{pert}}^q\rangle\rangle^{\otimes r}. \quad (29)$$

where  $\lambda_1, \dots, \lambda_{|\mathcal{C}|}$  are eigenvalues of  $\text{ad}_{H_{\text{pri}}^q}$  and

$$I(\lambda_{i_1}, \dots, \lambda_{i_r}) = \int_0^{T_{\text{seq}}} dt_1 \cdots \int_0^{t_{r-1}} dt_r e^{-i\lambda_{i_1} t_1} \cdots e^{-i\lambda_{i_r} t_r}. \quad (30)$$

The above integrals admit closed-form analytic expressions, which can be precomputed and stored to avoid repeated numerical integration. The diagonalization of  $\text{ad}_{H_{\text{pri}}^q}$  can be found using numerical Lanczos method.

### B. $\mathcal{C}$ -integrals of a shaped pulse

Denote the  $\mathcal{C}$ -integral of the  $q$ th step by  $\vec{c}^{(r-1)}(q)$ . Define

$$\vec{c}_{\text{tog}}^{(r-1)}(q) = [\mathcal{D}(U_1^\dagger) \cdots \mathcal{D}(U_{q-1}^\dagger)]^{\otimes r} \cdot \vec{c}^{(r-1)}(q), \quad (31)$$

where  $U_q$  is the primary unitary of the  $q$ th step. Then

$$\vec{c}^{(r-1)} = \sum_{r_1 + \dots + r_v = r} \sum_{Q \geq q_1 > \dots > q_v \geq 1} \vec{c}_{\text{tog}}^{(r_1-1)}(q_1) \otimes \vec{c}_{\text{tog}}^{(r_2-1)}(q_2) \otimes \cdots \otimes \vec{c}_{\text{tog}}^{(r_v-1)}(q_v). \quad (32)$$

For  $r = 1, 2$  and  $3$ , we have

$$\begin{aligned}
\bar{c}^{(0)} &= \sum_{q=1}^Q \bar{c}_{\text{tog}}^{(0)}(q), \\
\bar{c}^{(1)} &= \sum_{q=1}^Q \bar{c}_{\text{tog}}^{(1)}(q) + \sum_{q_1=2}^Q \sum_{q_2=1}^{q_1-1} \bar{c}_{\text{tog}}^{(0)}(q_1) \otimes \bar{c}_{\text{tog}}^{(0)}(q_2), \\
c^{(2)} &= \sum_{q=1}^Q \bar{c}_{\text{tog}}^{(2)}(q) + \sum_{q_1=2}^Q \sum_{q_2=1}^{q_1-1} \left[ \bar{c}_{\text{tog}}^{(0)}(q_1) \otimes \bar{c}_{\text{tog}}^{(1)}(q_2) + \bar{c}_{\text{tog}}^{(1)}(q_1) \otimes \bar{c}_{\text{tog}}^{(0)}(q_2) \right] + \sum_{q_1=3}^Q \sum_{q_2=2}^{q_1-1} \sum_{q_3=1}^{q_2-1} c_{\text{tog}}^{(0)}(q_1) \otimes c_{\text{tog}}^{(0)}(q_2) \otimes c_{\text{tog}}^{(0)}(q_3).
\end{aligned} \tag{33}$$

### C. Cross $\mathcal{C}$ -integrals

Eq. (32) can be generalized to cross  $\mathcal{C}$ -integrals that are defined on different spaces. In particular,

$$\begin{aligned}
\bar{c}_{\text{cross}}^{(1)} &= \int_0^{T_{\text{seq}}} dt_1 \int_0^{t_1} dt_2 \mathcal{D}_{\text{pert}}(U_{\text{pri}}^\dagger(t_1)) \otimes \mathcal{D}_{\text{err}}(U_{\text{pri}}^\dagger(t_2)) |H_{\text{pert}}\rangle\rangle_{\text{pert}} \otimes |A\rangle\rangle_{\text{err}} \\
&= \sum_{q_1=1}^Q \bar{c}_{\text{cross}}^{(1)}(q_1) + \sum_{q_1=2}^Q \sum_{q_2=1}^{q_1-1} \bar{c}_{\text{pert}}^{(0)}(q_1) \otimes \bar{c}_{\text{err}}^{(0)}(q_2),
\end{aligned} \tag{34}$$

where  $A$  is an error Hamiltonian, e.g.,  $\partial_j \Delta H$  and  $\partial_{j_1} \partial_{j_2} \Delta H$  (defined below). This is used in the calculation of the left-hand side of Eq. (59).

## V. ROBUSTNESS AGAINST CONTROL ERRORS

This section develops the general method for achieving control robustness. The conditions for achieving robustness will be expressed in terms of the  $\mathcal{C}$ -integrals.

When the model parameters  $\bar{\mu} = \{\mu_j\}$  are subject to variations  $\bar{\epsilon}$ , the total Hamiltonian is

$$H_{\text{tot}}(t) = H_c(t, \bar{\mu}) + \Delta H(t, \bar{\epsilon}) + H_{\text{int}}, \tag{35}$$

where

$$\Delta H(t, \bar{\epsilon}) = H_c(t, \bar{\mu} + \bar{\epsilon}) - H_c(t, \bar{\mu}), \tag{36}$$

and  $\Delta H(t, \vec{0}) = 0$ . The total unitary propagator becomes

$$U(T_{\text{seq}}, \bar{\epsilon}) = U_{\text{pri}}(T_{\text{seq}}) \mathcal{T} \exp \left[ -i \int_0^{T_{\text{seq}}} (\Delta H_{\text{tog}}(t, \bar{\epsilon}) + H_{\text{tog}}(t)) dt \right], \tag{37}$$

where

$$\begin{aligned}
\Delta H_{\text{tog}}(t, \bar{\epsilon}) &= U_{\text{pri}}^\dagger(t) \Delta H(t, \bar{\epsilon}) U_{\text{pri}}(t), \\
H_{\text{tog}}(t) &= U_{\text{pri}}^\dagger(t) H_{\text{pert}} U_{\text{pri}}(t).
\end{aligned} \tag{38}$$

Applying toggling-frame transformation under  $\Delta H_{\text{tog}}$  to the second factor of Eq. (37), we have

$$U(T_{\text{seq}}, \bar{\epsilon}) = U_{\text{pri}}(T_{\text{seq}}) U_{\text{err}}(T_{\text{seq}}, \bar{\epsilon}) \mathcal{T} \exp \left( -i \int_0^{T_{\text{seq}}} \tilde{H}_{\text{tog}}(t, \bar{\epsilon}) dt \right), \tag{39}$$

where

$$U_{\text{err}}(T_{\text{seq}}, \bar{\epsilon}) = \mathcal{T} \exp \left[ -i \int_0^{T_{\text{seq}}} \Delta H_{\text{tog}}(t, \bar{\epsilon}) dt \right] \tag{40}$$

and

$$\tilde{H}_{\text{tog}}(t, \vec{\epsilon}) = U_{\text{err}}^\dagger(t, \vec{\epsilon}) U_{\text{pri}}^\dagger(t) H_{\text{pert}} U_{\text{pri}}(t) U_{\text{err}}(t, \vec{\epsilon}). \quad (41)$$

Define the imperfect primary and perturbative unitary propagators as

$$\begin{aligned} \tilde{U}_{\text{pri}}(t, \vec{\epsilon}) &= U_{\text{pri}}(t) U_{\text{err}}(t, \vec{\epsilon}), \\ \tilde{U}_{\text{pert}}(t, \vec{\epsilon}) &= \mathcal{T} \exp\left(-i \int_0^{T_{\text{seq}}} \tilde{H}_{\text{tog}}(t, \vec{\epsilon}) dt\right), \end{aligned} \quad (42)$$

we have

$$U(T_{\text{seq}}, \vec{\epsilon}) = \tilde{U}_{\text{pri}}(T_{\text{seq}}, \vec{\epsilon}) \tilde{U}_{\text{pert}}(T_{\text{seq}}, \vec{\epsilon}). \quad (43)$$

We want to achieve robustness for both the primary and perturbative unitary propagators independently

$$\tilde{U}_{\text{pri}}(T_{\text{seq}}, \vec{\epsilon}) = U_{\text{target}} + O(\vec{\epsilon}^{n+1}) \quad (44)$$

and

$$\tilde{U}_{\text{pert}}(t, \vec{\epsilon}) = \exp(-i H_{\text{target}} T_{\text{seq}}) + O(\vec{\epsilon}^{n+1}). \quad (45)$$

Together, they achieve the  $n$ th-order robustness in  $U(T_{\text{seq}})$ :

$$U(T_{\text{seq}}, \vec{\epsilon}) = U_{\text{target}} \exp(-i H_{\text{target}} T_{\text{seq}}) + O(\vec{\epsilon}^{n+1}). \quad (46)$$

Next, we will discuss how to achieve Eqs. (44) and (45) individually.

### A. Robustness in $U_{\text{pri}}(T_{\text{seq}})$

Represent the error unitary (Eq. (40)) by an effective Hamiltonian  $H_{\text{err}}$

$$U_{\text{err}}(T_{\text{seq}}, \vec{\epsilon}) = \exp(-i H_{\text{err}} T_{\text{seq}}), \quad (47)$$

where  $H_{\text{err}}$  can be calculated using the Magnus expansion  $H_{\text{err}} = \sum_{i=0}^{\infty} \bar{H}_{\text{err}}^{(i)}$

$$\begin{aligned} \bar{H}_{\text{err}}^{(0)} &= \frac{1}{T_{\text{seq}}} \int_0^{T_{\text{seq}}} \Delta H_{\text{tog}}(t_1) dt_1, \\ \bar{H}_{\text{err}}^{(1)} &= -\frac{i}{2T_{\text{seq}}} \int_0^{T_{\text{seq}}} dt_1 \int_0^{t_1} dt_2 [\Delta H_{\text{tog}}(t_1), \Delta H_{\text{tog}}(t_2)] \\ &\dots \end{aligned} \quad (48)$$

Denote

$$\partial_{j_1} \dots \partial_{j_i} \Delta H_{\text{tog}} = \left. \frac{\partial^i}{\partial \mu_{j_1} \dots \partial \mu_{j_i}} \Delta H_{\text{tog}} \right|_{\vec{\epsilon}=\vec{0}}. \quad (49)$$

The robustness is achieved by requiring

$$\begin{aligned} \frac{1}{T_{\text{seq}}} \int_0^{T_{\text{seq}}} \partial_{j_1} \Delta H_{\text{tog}}(t) dt &= 0, \\ \frac{1}{T_{\text{seq}}} \int_0^{T_{\text{seq}}} \partial_{j_1} \partial_{j_2} \Delta H_{\text{tog}}(t) dt &= 0, \\ -\frac{i}{2T_{\text{seq}}} \int_0^{T_{\text{seq}}} dt_1 \int_0^{t_1} dt_2 [\partial_{j_1} \Delta H_{\text{tog}}(t_1), \partial_{j_2} \Delta H_{\text{tog}}(t_2)] &= 0, \\ &\dots \end{aligned} \quad (50)$$

In  $\mathcal{C}_{\text{err}}(\mathbf{g}_{\text{pri}}, \Delta H)$ , the time-ordered  $\mathcal{C}$ -integrals corresponding to the conditions (50) are

$$\bar{c}^{(0)}(\partial_{j_1} \Delta H), \quad \bar{c}^{(0)}(\partial_{j_1} \partial_{j_2} \Delta H), \quad \bar{c}^{(1)}(\{\partial_{j_1} \Delta H(t, \vec{0}), \partial_{j_2} \Delta H\}), \quad \dots, \quad (51)$$

where the  $\mathcal{C}$ -integrals are defined as

$$\bar{c}^{(r-1)}(\{A_1, \dots, A_r\}) = \int_0^{T_{\text{seq}}} dt_1 \dots \int_0^{t_{r-1}} dt_r \mathcal{D}(U_{\text{pri}}^\dagger)(t_1) \otimes \dots \otimes \mathcal{D}(U_{\text{pri}}^\dagger)(t_r) |A_1(t_1)\rangle \otimes \dots \otimes |A_r(t_r)\rangle. \quad (52)$$

The corresponding robustness conditions are

$$\begin{aligned} |\bar{c}^{(0)}(\partial_{j_1} \Delta H)| &= 0, & |\bar{c}^{(0)}(\partial_{j_1} \partial_{j_2} \Delta H)| &= 0, \\ |\bar{c}_{i_1 i_2}(\{\partial_{j_1} \Delta H, \partial_{j_2} \Delta H\}) + \bar{c}_{i_2 i_1}(\{\partial_{j_1} \Delta H, \partial_{j_2} \Delta H\})| &= 0. \end{aligned} \quad (53)$$

### B. Robustness in $U_{\text{pert}}(T_{\text{seq}})$

Representing the imperfect toggling-frame Hamiltonian  $\tilde{H}_{\text{tog}}(t, \vec{\epsilon})$  (Eq. (41)) in  $\mathcal{C}_{\text{pert}}(\mathbf{g}_{\text{pri}}, H_{\text{pert}})$ , we have

$$|\tilde{H}_{\text{tog}}(t)\rangle_{\text{pert}} = \mathcal{D}_{\text{pert}}(U_{\text{err}}^\dagger(t, \vec{\epsilon})) |H_{\text{tog}}(t)\rangle_{\text{pert}}. \quad (54)$$

Applying the Dyson expansion to  $U_{\text{err}}^\dagger(t, \vec{\epsilon})$  (Eq. (40)) yields

$$\mathbb{D}_{\text{pert}}(U_{\text{err}}^\dagger(t, \vec{\epsilon})) = \mathbb{1} + i \int_0^t \mathcal{D}_{\text{pert}}(\text{ad}_{\Delta H_{\text{tog}}}(t_1, \vec{\epsilon})) dt_1 + \dots \quad (55)$$

Expand  $\Delta H$  to the first order of  $\vec{\epsilon}$ , we obtain

$$\mathbb{D}_{\text{pert}}(U_{\text{err}}^\dagger(t, \vec{\epsilon})) = \mathbb{1} + i \int_0^t \mathcal{D}_{\text{pert}}[\vec{\epsilon} \cdot \vec{\partial}(\text{ad}_{\Delta H_{\text{tog}}}(t_1, \vec{0}))] dt_1 + O(\vec{\epsilon}^2). \quad (56)$$

Substituting it into  $\bar{c}^{(0)}$  gives

$$\begin{aligned} \bar{c}^{(0)} &= \int_0^{T_{\text{seq}}} dt_1 \mathcal{D}_{\text{pert}}(U_{\text{err}}^\dagger(t_1, \vec{\epsilon})) |H_{\text{tog}}(t_1)\rangle_{\text{pert}} \\ &= \int_0^{T_{\text{seq}}} dt_1 |H_{\text{tog}}(t_1)\rangle_{\text{pert}} + i \int_0^{T_{\text{seq}}} dt_1 \int_0^{t_1} dt_2 \mathcal{D}_{\text{pert}}[\vec{\epsilon} \cdot \vec{\partial}(\text{ad}_{\Delta H_{\text{tog}}}(t_2, \vec{0}))] |H_{\text{tog}}(t_1)\rangle_{\text{pert}} + O(\vec{\epsilon}^2). \end{aligned} \quad (57)$$

The leading term of the error (in  $\bar{c}^{(0)}$ ) is removed by requiring

$$\int_0^{T_{\text{seq}}} dt_1 \int_0^{t_1} dt_2 \mathcal{D}_{\text{pert}}[\partial_j(\text{ad}_{\Delta H_{\text{tog}}}(t_2, \vec{0}))] |H_{\text{tog}}(t_1)\rangle_{\text{pert}} = 0, \quad (58)$$

for all  $j = 1, \dots, J$ . Since  $\partial_j \Delta H_{\text{tog}}(t) = \sum_{l=1}^{|\mathcal{C}_{\text{err}}|} c_l^{\text{err}}(t; \partial_j \Delta H) h_{\text{err}}^l$  and  $H_{\text{tog}}(t) = \sum_{s=1}^{|\mathcal{C}_{\text{pert}}|} c_s^{\text{pert}}(t) h_{\text{pert}}^s$  where  $\{h_{\text{err}}^l\}$  and  $\{h_{\text{pert}}^s\}$  are the bases of their corresponding spaces, the above condition becomes

$$\left\| \sum_{l=1}^{|\mathcal{C}_{\text{err}}|} \sum_{s=1}^{|\mathcal{C}_{\text{pert}}|} \int_0^{T_{\text{seq}}} dt_1 \int_0^{t_1} dt_2 c_l^{\text{err}}(t_2; \partial_j \Delta H) c_s^{\text{pert}}(t_1) [h_{\text{err}}^l, h_{\text{pert}}^s] \right\| = 0. \quad (59)$$

Higher-order corrections can be incorporated by considering  $\bar{c}^{(1)}, \bar{c}^{(2)}, \dots$  and retaining higher-order terms in the Dyson and Taylor expansions.

### C. Control Robustness is Always Achievable

In the presence of an error Hamiltonian  $\Delta H(t, \mu + \epsilon)$ , assume the following: (1) there exists an implementation of the identity operator that is robust to  $\epsilon$  to at least zeroth order (e.g., a waiting period where  $a_k(t) \equiv 0$ ); (2)  $\Delta H$  continuously depends on  $a_k(t)$  and  $\mu$ ; and (3) the correlation time of  $\Delta H$  is finite so that we can compose gates

without interference, then the following result holds when single-qubit universal control is available.

**Theorem V.1.** *Zeroth-order robustness to  $\epsilon$  is always achievable to any systematic error Hamiltonian  $\Delta H$ .*

*Proof.* The total Hamiltonian is

$$H_{\text{tot}}(t) = H_c(t) + \epsilon \frac{\partial}{\partial \epsilon} \Delta H(t, 0) + O(\epsilon^2). \quad (60)$$

The goal is to design a unitary  $U_{\text{target}}$  so that

$$\begin{aligned} U(T_{\text{seq}}, 0) &= U_{\text{target}}, \\ U(T_{\text{seq}}, \epsilon) &= U_{\text{target}} + O(\epsilon^2). \end{aligned} \quad (61)$$

Suppose that we have found a sequence  $U_0(T_{\text{seq}}, \epsilon)$  that achieves the first condition in Eqs. (61). In general,

$$U_0(T_{\text{seq}}, \epsilon) = U_{\text{target}} e^{-i\epsilon\sigma_0\theta} + O(\epsilon^2). \quad (62)$$

If we could implement a sequence  $U^*$  so that

$$U^*(T_{\text{seq}}, \epsilon) = e^{i\epsilon\sigma_0\theta} + O(\epsilon^2), \quad (63)$$

then  $U_0 U^*$  achieves a robust implementation of  $U_{\text{target}}$  in zeroth order.

Let  $U_1 = \mathbb{1} + O(\epsilon^2)$  and  $U_2 = \mathbb{1} + O(\epsilon)$ . Since we can continuously modify  $U_1$  into  $U_2$ , there exists  $U_r = \exp(-ir\epsilon\sigma') + O(\epsilon^2)$ ,  $\forall r > 0$  and some  $\sigma'$ . Therefore, if we choose  $r$  small enough, we can achieve  $U_r^N \approx \exp(-ise\sigma') + O(\epsilon^2)$  to arbitrary accuracy,  $\forall s > 0$  and some positive integer  $N$ .

Due to universal control, we can rotate  $\sigma'$  to any direction. Thus, we can implement  $U_\alpha(s) = \exp(-i(s\epsilon\sigma_\alpha + \epsilon\sigma_{r_\alpha})) + O(\epsilon^2)$ , for  $\alpha = \pm x, \pm y$  and  $\pm z$ . Here,  $\sigma_{r_\alpha}$  corresponds to the error introduced by the imperfect rotation. Since we can choose any  $s > 0$  and  $\sigma_{r_\alpha}$  does not depend on  $s$ , therefore,  $\forall \sigma_0, \exists s_\alpha > 0$  so that  $\prod_\alpha U_\alpha(s_\alpha) = e^{i\epsilon\sigma_0\theta} + O(\epsilon^2)$ .  $\square$

The result is a generalization of the result from [5]. All the errors considered in this work (Rabi field variation, variations in linear or nonlinear models) satisfy the assumptions and therefore can be corrected to at least zeroth order. Additionally, requiring control robustness does not affect the controllability of  $U_{\text{pri}}$  or  $U_{\text{pert}}$ , so when characterizing the achievable sets of  $U_{\text{target}}$  and  $H_{\text{target}}$ , we do not need to consider  $\Delta H$ .

## VI. HIGHER-ORDER CORRECTIONS

Having structured the control and internal Hamiltonian such that the desired effective Hamiltonian is achievable in zeroth order, the remaining task is to engineer the average Hamiltonian of higher orders to be under a threshold, which needs to be accomplished for the entire distributions of Hamiltonian parameters. This is necessary for achieving high precision when the target control is achieved through the effective Hamiltonian.

Although, the frequency of modulation is typically much larger than  $\|H_{\text{pert}}\|$ , making  $\bar{H}^{(n)} \sim (H_{\text{pert}}\tau_c)^{n+1}/T_{\text{seq}}$  a small quantity of order  $n+1$ , where  $\tau_c$  is the characteristic time of the modulation [6, 7], modulation of controls can lead to higher-order terms being larger than low-order terms.

It is well-known that odd-order correction terms can be eliminated by symmetrizing the control sequence [8]. This is widely used for decoupling and is straightforward to implement for simulations. When  $H_{\text{pri}}$  contains  $H_{\text{int}}$ , however, a sequence cannot be symmetrized in general, since the sign of  $H_{\text{int}}$  cannot be reversed. Here, we provide computable conditions in terms of the  $\mathcal{C}$ -integrals.

The higher-order correction terms in the Magnus expansion are

$$\begin{aligned} \bar{H}^{(1)} &= -\frac{i}{2T_{\text{seq}}} \int_0^{T_{\text{seq}}} dt_1 \int_0^{t_1} dt_2 [H_{\text{tog}}(t_1), H_{\text{tog}}(t_2)], \\ \bar{H}^{(2)} &= -\frac{1}{6T_{\text{seq}}} \int_0^{T_{\text{seq}}} dt_1 \int_0^{t_1} dt_2 \int_0^{t_2} dt_3 ([H_{\text{tog}}(t_1), [H_{\text{tog}}(t_2), H_{\text{tog}}(t_3)]] + [H_{\text{tog}}(t_2), [H_{\text{tog}}(t_2), H_{\text{tog}}(t_1)]]), \\ &\dots \end{aligned} \quad (64)$$

Denote

$$\begin{aligned} F_2(A_1, A_2) &= [A_1, A_2], \\ F_3(A_1, A_2, A_3) &= [A_1, [A_2, A_3]] + [A_3, [A_2, A_1]], \\ &\dots, \end{aligned} \tag{65}$$

then  $F_r(A_1, \dots, A_r) = (-1)^{r-1} F_r(A_r, \dots, A_1)$ . Represent  $H_{\text{tog}}(t)$  in  $\mathcal{C}(\mathbf{g}_{\text{pri}}, H_{\text{pert}})$ , we have

$$F_r(H_{\text{tog}}(t_1), \dots, H_{\text{tog}}(t_r)) = \sum_{i_1, \dots, i_r=1}^{|\mathcal{C}|} c_{i_1}(t_1) \dots c_{i_r}(t_r) F_r(h_{i_1}, \dots, h_{i_r}). \tag{66}$$

Therefore, since the  $(r-1)$ th correction term is

$$\bar{H}^{(r-1)} \propto \int_0^{T_{\text{seq}}} dt_1 \dots \int_0^{t_{r-1}} dt_r F_r(H_{\text{tog}}(t_1), \dots, H_{\text{tog}}(t_r)), \tag{67}$$

the condition for  $\bar{H}^{(r-1)} \equiv 0$  for all  $h_1, \dots, h_r$  is given by

$$|\bar{c}_{i_1 \dots i_r}(T_{\text{seq}}) - (-1)^{r-1} \bar{c}_{i_r \dots i_1}(T_{\text{seq}})| = 0, \tag{68}$$

for all  $i_1, \dots, i_r$  excluding the situations where  $i_1 = \dots = i_r$ .

## VII. NUMERICAL SETUP FOR SEQUENCE DESIGN

The objectives of a control sequence include achieving a target primary unitary, engineering a desired zeroth-order average Hamiltonian while accounting for higher-order corrections, and satisfying robustness requirements. Table I summarizes these goals. The criteria of the objectives take the form

TABLE I: Conditions for achieving different objectives.

Objective name	Subject	Target	Criterion
Primary unitary	$U_{\text{pri}}(T_{\text{seq}})$	$U_{\text{target}}$	$1 - \frac{ \text{Tr}(U_{\text{pri}} U_{\text{target}}^\dagger) }{\text{Tr}(U_{\text{target}} U_{\text{target}}^\dagger)} = 0$
First-order primary robustness	$\partial_j \Delta \bar{H}(t, \vec{0})$	0	Eq. 1 of (53)
Second-order primary robustness	$\partial_{j_1} \partial_{j_2} \Delta H(t, \vec{0})$	0	Eq. 2 of (53)
First-order cross primary robustness	$\partial_{j_1} \Delta H(t, \vec{0}), \partial_{j_2} \Delta H(t, \vec{0})$	0	Eq. 3 of (53)
Zero-order average Hamiltonian	$\bar{H}^{(0)}(T_{\text{seq}})$	$H_{\text{target}}$	$ \bar{c}^{(0)} -  H_{\text{target}}   = 0$
$(r-1)$ th-order correction ( $r > 1$ )	$\bar{H}^{(r-1)}(T_{\text{seq}})$	0	Eq. (68)
First-order effective Hamiltonian robustness	$\partial_j \Delta H(t), H_{\text{tog}}(t)$	0	Eq. (59)

$$f(\text{sequence, objective}) = 0 \tag{69}$$

where  $f$  is a positive function of the sequence and the objective. Therefore, the total cost function (the objective function is just 1-the cost function) can be written as

$$f_{\text{tot}}(\{a_k(t)\}) = \sum_i w_i f_i, \tag{70}$$

where  $f_i$  is the function value of  $f$  of the  $i$ th objective and  $w_i$  are positive weights. One can adjust the weight to reflect the difference in importance of different objectives. All the objectives are met when  $f_{\text{tot}}(\{a_k(t)\}) = 0$ . Therefore, the task of designing a sequence is an optimization (minimization of the cost function) problem whose goal is to find  $\{a_k(t)\}$  that minimizes  $f_{\text{tot}}(\{a_k(t)\})$ .

---

**Algorithm 4** Generalized simulated annealing. For a fixed  $q_a \in \mathbb{R}$ , a fixed  $1 < q_v < 3$ , an initial temperature  $T_0$ , a maximal number of iterations  $t_{\max}$ , the function GSA takes an  $D$ -dimensional Energy function  $E$ , an initial guess  $\vec{x}_1$  and the target energy value  $E_{\text{target}}$  as input and return a solution  $\vec{x}_{\text{best}}$  such that either  $E(\vec{x}_{\text{best}}) < E_{\text{target}}$  or that is the best solution found within maximal number of iterations.

---

```

1: function TSALLISRNG( $T$ )
2:    $p \leftarrow \frac{3-q_v}{2(q_v-1)}$ 
3:    $s \leftarrow \frac{\sqrt{2(q_v-1)}}{(T)^{1/(3-q_v)}}$ 
4:   Generate iid  $x_i \sim \mathcal{N}(0, 1)$  for  $i = 1, 2, \dots, D$ 
5:    $\vec{x} \leftarrow (x_1, x_2, \dots, x_D)$ 
6:   Generate a gamma random number  $u \sim \gamma(1, p)$ 
7:   return  $\frac{\vec{x}}{s\sqrt{u}}$ 
8: end function
9: function TEMPERATURE( $t$ )
10:  return  $\frac{(q_v-1)^{2-1} T_0}{(q_v-1)^{t+1}-1}$ 
11: end function
12: function COMPAREENERGY( $E_1, E_2, T$ )
13:   $r \leftarrow$  random real number from  $[0, 1]$ 
14:   $a \leftarrow 1 + \frac{(E_2-E_1)(q_a-1)}{T}$ 
15:   $b \leftarrow \left[ 1 + \frac{(E_2-E_1)(q_a-1)}{T} \right]^{-\frac{1}{q_a-1}}$ 
16:  if  $E_2 < E_1$  then
17:    return True
18:  else
19:    if  $q_a > 1$  then
20:      return Boole( $r \leq b$ )
21:    else if  $q_a < 1$  then
22:      return Boole( $a \geq 0$  and  $r \leq b$ )
23:    else
24:      return Boole( $r \leq \exp[(E_1 - E_2)/T]$ )
25:    end if
26:  end if
27: end function
28: function GSA( $E, \vec{x}_1$ )
29:   $E_1 \leftarrow E(\vec{x}_1)$ 
30:   $E_{\text{best}} \leftarrow E_1$ 
31:   $\vec{x}_{\text{best}} \leftarrow \vec{x}_1$ 
32:   $t \leftarrow 1$ 
33:  while  $t < t_{\max}$  and  $E_{\text{best}} > E_{\text{target}}$  do
34:     $T \leftarrow$  TEMPERATURE( $t$ )
35:     $\vec{x}_2 \leftarrow$  LEGALIZE( $\vec{x}_1 +$  TSALLISRNG( $T$ ))
36:     $E_2 \leftarrow E(\vec{x}_2)$ 
37:    if  $E_2 < E_{\text{best}}$  then
38:       $E_{\text{best}} \leftarrow E_2$ 
39:       $\vec{x}_{\text{best}} \leftarrow \vec{x}_2$ 
40:    end if
41:    if COMPAREENERGY( $E_1, E_2, T$ ) then
42:       $\vec{x}_1 \leftarrow \vec{x}_2$ 
43:       $E_1 \leftarrow E_2$ 
44:    end if
45:     $t \leftarrow t + 1$ 
46:  end while
47:  return  $\vec{x}_{\text{best}}$ 
48: end function

```

---

## VIII. OPTIMIZATION ALGORITHMS

Algorithm 4 is the pseudocode of the generalized simulated annealing [9] for sequence optimization. A  $D$ -dimensional Tsallis random number generator introduced in [10] is used. For best efficiency, the best solution should always be stored [11].

The legalizer that restricts the parameters within  $[-1, 1]$  is defined through

$$B(x) = (-1)^{\lfloor \frac{x+1}{2} \rfloor} \left( x - 2 \left\lfloor \frac{x+1}{2} \right\rfloor \right), \quad (71)$$

and

$$F(\bar{x}) = f(B(\bar{x})). \quad (72)$$

To find optimized hyperparameters ( $T_0$ ,  $q_v$  and  $q_a$ ), test runs are implemented on trial problems with fixed  $i_{\max}$ , then a Nelder-Mead optimizer [12, 13] is used to adjust  $T_0$ ,  $q_v$  and  $q_a$  to optimize the average performance [14]. Additionally, parallel searches [15] are implemented to increase efficiency.

## IX. ROBUST CONTROL IN NONLINEAR SYSTEMS

Start with the state-space equation

$$\frac{d\vec{B}}{dt} = h(\vec{B}, \vec{a}, t; \vec{\mu}_0), \quad (73)$$

a variation  $\vec{\epsilon}$  in the model parameter  $\vec{\mu}$  results in a different output field  $\vec{B}(t, \vec{\mu}_0 + \vec{\epsilon}) = \vec{B}(t, \vec{\mu}_0) + \sum_i \epsilon_i \frac{\partial \vec{B}}{\partial \mu_i}(t, \vec{\mu}_0) + \dots$ . The differential equation becomes

$$\frac{d}{dt} \left( \vec{B} + \sum_i \epsilon_i \frac{\partial \vec{B}}{\partial \mu_i} + \dots \right) = h(\vec{B}(\vec{\mu}_0), \vec{a}, t; \vec{\mu}_0) + \sum_i \epsilon_i \mathbf{J}(h, \vec{B})|_{\vec{\mu}=\vec{\mu}_0} \frac{\partial \vec{B}}{\partial \epsilon_i}(\vec{\mu}_0) + \dots, \quad (74)$$

where  $\mathbf{J}$  is the Jacobian matrix. By equating terms of the same order in  $\epsilon_i$ , we can obtain coupled differential equations that can be solved for  $\frac{\partial \vec{B}}{\partial \mu_i}, \dots$ , enabling evaluation of the error Hamiltonian  $\Delta H$ . For the resonant circuit in Fig. 5.

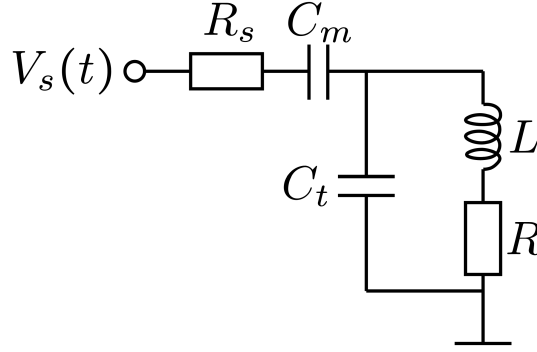


FIG. 5: A simple resonant circuit with  $R_s = 50 \Omega$ ,  $R = 0.01 \Omega$ ,  $C_m = 11 \text{ fF}$ ,  $C_t = 1.479 \text{ pF}$ , and  $L = 170 \text{ pH}$ . The resonance frequency is around 10 GHz. We choose  $\kappa_i = 1 \text{ V}^{-1}$  and  $\kappa_o = 2 \text{ A}^{-1}$ .

In a rotating frame of frequency  $\omega_r$ , it obeys the following differential equation [16]

$$\frac{dx}{dt} = A(x)x + \alpha(t)u, \quad (75)$$

where

$$x = \begin{pmatrix} \tilde{I}_L \\ \tilde{V}_{C_m} \\ \tilde{V}_{C_t} \end{pmatrix}, \quad A(x) = \begin{pmatrix} -\frac{R}{L} & 0 & \frac{1}{L} \\ 0 & \frac{-1}{R_L C_m} & \frac{1}{R_L C_m} \\ -\frac{1}{C_t} & \frac{-1}{R_L C_t} & \frac{1}{R_L C_t} \end{pmatrix} - i\omega_r \mathbb{1}, \quad u = \begin{pmatrix} 0 \\ \frac{1}{R_L C_m} \\ \frac{1}{R_L C_t} \end{pmatrix}, \quad (76)$$

and

$$a_1(t) = \kappa_i \text{Re}(\alpha(t)), \quad a_2(t) = \kappa_i \text{Im}(\alpha(t)), \quad b_1(t) = \kappa_o \text{Re}(\tilde{I}_L), \quad b_2(t) = \kappa_o \text{Im}(\tilde{I}_L), \quad (77)$$

where  $\kappa_i$  and  $\kappa_o$  are normalization constants that depend on the geometry of the control system.

In the presence of kinetic inductance, the value of  $L$  depends on the current:

$$L = L_0(1 + \alpha_L |I_L|^2), \quad (78)$$

where  $\alpha_L$  is a constant. We want to design for  $\alpha_L = 0$  and to achieve robustness for small  $\alpha_L$ . Using Eq. (74), the equations for  $x(\alpha_L = 0)$  and  $\frac{\partial x}{\partial \alpha_L}(\alpha_L = 0)$  are

$$\frac{d}{dt} \begin{pmatrix} x \\ \frac{\partial x}{\partial \alpha_L} \end{pmatrix} = \begin{pmatrix} A(x) & 0 \\ \frac{\partial A}{\partial \alpha_L}(x) & A(x) \end{pmatrix} \begin{pmatrix} x \\ \frac{\partial x}{\partial \alpha_L} \end{pmatrix} + \alpha(t) \begin{pmatrix} u \\ \frac{\partial u}{\partial \alpha_L} \end{pmatrix} \Big|_{\alpha_L=0}, \quad (79)$$

where

$$\frac{\partial A}{\partial \alpha_L}(x, \alpha_L = 0) = \begin{pmatrix} \frac{R|\tilde{I}_L|^2}{L_0} & 0 & -\frac{|\tilde{I}_L|^2}{L_0} \\ 0 & 0 & 0 \\ 0 & 0 & 0 \end{pmatrix}, \quad \frac{\partial u}{\partial \alpha_L} = 0. \quad (80)$$

The distortion of the input pulse and the corresponding error Hamiltonian are thus calculated by solving the system of differential equations.

- 
- [1] F. Mezzadri, How to generate random matrices from the classical compact groups, arXiv preprint math-ph/0609050 (2006).
  - [2] G. F. Lawler and V. Limic, *Random walk: a modern introduction*, Vol. 123 (Cambridge University Press, 2010).
  - [3] C. B. Barber, D. P. Dobkin, and H. Huhdanpaa, The quickhull algorithm for convex hulls, *ACM Transactions on Mathematical Software (TOMS)* **22**, 469 (1996).
  - [4] P. Virtanen, R. Gommers, T. E. Oliphant, M. Haberland, T. Reddy, D. Cournapeau, E. Burovski, P. Peterson, W. Weckesser, J. Bright, *et al.*, Scipy 1.0: fundamental algorithms for scientific computing in python, *Nature methods* **17**, 261 (2020).
  - [5] K. R. Brown, A. W. Harrow, and I. L. Chuang, Arbitrarily accurate composite pulse sequences, *Physical Review A—Atomic, Molecular, and Optical Physics* **70**, 052318 (2004).
  - [6] U. Haeberlen and J. S. Waugh, Coherent averaging effects in magnetic resonance, *Physical Review* **175**, 453 (1968).
  - [7] M. M. Maricq, Application of average hamiltonian theory to the nmr of solids, *Physical Review B* **25**, 6622 (1982).
  - [8] P. Mansfield, Symmetrized pulse sequences in high resolution nmr in solids, *Journal of Physics C: Solid State Physics* **4**, 1444 (1971).
  - [9] C. Tsallis and D. A. Stariolo, Generalized simulated annealing, *Physica A: Statistical Mechanics and its Applications* **233**, 395 (1996).
  - [10] T. Schanze, An exact d-dimensional tsallis random number generator for generalized simulated annealing, *Computer physics communications* **175**, 708 (2006).
  - [11] R. W. Eglese, Simulated annealing: a tool for operational research, *European journal of operational research* **46**, 271 (1990).
  - [12] J. A. Nelder and R. Mead, A simplex method for function minimization, *The computer journal* **7**, 308 (1965).
  - [13] J. C. Lagarias, J. A. Reeds, M. H. Wright, and P. E. Wright, Convergence properties of the nelder–mead simplex method in low dimensions, *SIAM Journal on optimization* **9**, 112 (1998).
  - [14] M.-W. Park and Y.-D. Kim, A systematic procedure for setting parameters in simulated annealing algorithms, *Computers & Operations Research* **25**, 207 (1998).
  - [15] D. J. Ram, T. Sreenivas, and K. G. Subramaniam, Parallel simulated annealing algorithms, *Journal of parallel and distributed computing* **37**, 207 (1996).
  - [16] I. Hincks, C. Granade, T. W. Borneman, and D. G. Cory, Controlling quantum devices with nonlinear hardware, *Physical Review Applied* **4**, 024012 (2015).